



Defense Threat Reduction Agency
8725 John J. Kingman Road, MS 6201
Fort Belvoir, VA 22060-6201



DTRA-TR-03-26

TECHNICAL REPORT

Lithospheric Structure of the Arabian Shield from the Joint Inversion of Receiver Function and Surface-Wave Dispersion Observations

Approved for public release; distribution is unlimited.

April 2006

DSWA01-98-C-0160

J. Julia et al.

Prepared by:
Saint Louis University
Department of Earth and
Atmospheric Sciences
3507 Laclede Avenue
St. Louis, MO 63103

DARE Tracking
73771

DESTRUCTION NOTICE

FOR CLASSIFIED documents, follow the procedures in DoD 5550.22-M, National Industrial Security Program Operating Manual, Chapter 5, Section 7 (NISPOM) or DoD 5200.1-R, Information Security Program Regulation, Chapter 1X.

FOR UNCLASSIFIED limited documents, destroyed by any method that will prevent disclosure of contents or reconstruction of the document.

Retention of this document by DoD contractors is authorized in accordance with DoD 5220.22M, Industrial Security manual.

PLEASE NOTIFY THE DEFENSE THREAT REDUCTION AGENCY, ATTN: IMMI, 8725 JOHN J. KINGMAN ROAD, MS-6201, FT. BELVOIR, VA 22060-6201. IF YOUR ADDRESS IS INCORRECT, IF YOU WISH IT DELETED FROM THE DISTRIBUTION LIST, OR IF THE ADDRESSEE IS NO LONGER EMPLOYED BY YOUR ORGANIZATION.

DISTRIBUTION LIST UPDATE

This mailer is provided to enable DTRA to maintain current distribution lists for reports. (We would appreciate you providing the requested information.)

- Add the individual listed to your distribution list.
- Delete the cited organization/individual.
- Change of address.

Note:
Please return the mailing label from the document so that any additions, changes, corrections or deletions can be made easily. For distribution cancellation or more information call DTRA/BDLMI (703) 767-4725.

NAME: _____

ORGANIZATION: _____

OLD ADDRESS	NEW ADDRESS
_____	_____
_____	_____
_____	_____

TELEPHONE NUMBER: () _____

DTRA PUBLICATION NUMBER/TITLE	CHANGES/DELETIONS/ADDITONS, etc. <i>(Attach Sheet if more Space is Required)</i>
_____	_____
_____	_____
_____	_____

DTRA or other GOVERNMENT CONTRACT NUMBER: _____

CERTIFICATION of NEED-TO-KNOW BY GOVERNMENT SPONSOR (if other than DTRA):

SPONSORING ORGANIZATION: _____

CONTRACTING OFFICER or REPRESENTATIVE: _____

SIGNATURE: _____

DEFENSE THREAT REDUCTION AGENCY
ATTN: BDLMI
8725 John J Kingman Road, MS 6201
Fort Belvoir, VA 22060-6201

DEFENSE THREAT REDUCTION AGENCY
ATTN: BDLMI
8725 John J Kingman Road, MS 6201
Fort Belvoir, VA 22060-6201

REPORT DOCUMENTATION PAGE

Form Approved
OMB No. 0704-0188

Public reporting burden for this collection of information is estimated to average 1 hour per response, including the time for reviewing instructions, searching existing data sources, gathering and maintaining the data needed, and completing and reviewing this collection of information. Send comments regarding this burden estimate or any other aspect of this collection of information, including suggestions for reducing this burden to Department of Defense, Washington Headquarters Services, Directorate for Information Operations and Reports (0704-0188), 1215 Jefferson Davis Highway, Suite 1204, Arlington, VA 22202-4302. Respondents should be aware that notwithstanding any other provision of law, no person shall be subject to any penalty for failing to comply with a collection of information if it does not display a currently valid OMB control number. PLEASE DO NOT RETURN YOUR FORM TO THE ABOVE ADDRESS.

1. REPORT DATE (DD-MM-YYY) April 2006		2. REPORT TYPE Technical Report		3. DATES COVERED (From - To)	
4. TITLE AND SUBTITLE Lithospheric Structure of the Arabian Shield from the Joint Inversion of Receiver Function and Surface-Wave Dispersion Observations (U)				5a. CONTRACT NUMBER DSWA 01-98-C-0160	
				5b. GRANT NUMBER	
				5c. PROGRAM ELEMENT NUMBER 1310	
6. AUTHOR(S) Jordi Julia, Charles J. Ammon, and Robert B. Herrimann				5d. PROJECT NUMBER OS	
				5e. TASK NUMBER OO	
				5f. WORK UNIT NUMBER DH85355	
7. PERFORMING ORGANIZATION NAME(S) AND ADDRESS(ES) Saint Louis University Department of Earth and Atmospheric Sciences 3507 Laclede Avenue St. Louis, MO 63103				8. PERFORMING ORGANIZATION REPORT NUMBER	
9. SPONSORING / MONITORING AGENCY NAME(S) AND ADDRESS(ES) Defense Threat Reduction Agency 8725 John J. Kingman Rd., MS 6201 Fort Belvoir, VA 22060-6201				10. SPONSOR/MONITOR'S ACRONYM(S) DTRA	
				11. SPONSOR/MONITOR'S REPORT NOS. TR-03-26	
12. DISTRIBUTION / AVAILABILITY STATEMENT Approved for public release; distribution is unlimited.					
13. SUPPLEMENTARY NOTES This work was sponsored by the Defense Threat Reduction Agency under the RDT&E RMC Code B 1310 D 2B13 OS OO 85355 24904D.					
14. ABSTRACT We estimate lithospheric velocity structure for the Arabian shield by modeling receiver functions and Love and Rayleigh group velocities from events recorded by the 1995-1997 Saudi Arabian Portable Broadband Deployment. Receiver functions are primarily sensitive to shear-wave velocity contrasts and vertical travel times and surface-wave dispersion measurements are sensitive to vertical shear-wave velocity averages, so that their combination bridge resolution gaps associated with each individual data set. We incorporate depth-dependent smoothness constraints on the resulting velocity models utilizing a jumping inversion technique. Additional constraints for the upper mantle are placed during inversion to complement those provided in our dataset. Our results show a 32-36 km thick crust consisting of a 10-12 km thick upper crust containing a rapid velocity increase, a rather constant velocity lower crust 3.84(+0.04 km/s overlaid by a significant velocity gradient above 16-22 km depth. The upper mantle material is shown to have shear velocities ranging from 4.3 to 4.6 km/s and the crust-to-mantle transition is imaged as a gradational transition zone (4-12 km thick) rather than a sharp discontinuity. Evidence for lateral variations in both crust and upper mantle is observed at some stations, as well.					
15. SUBJECT TERMS Seismic Surface Waves Velocity Structure Arabian Plate Joint Inversion Receiver Functions					
16. SECURITY CLASSIFICATION OF:			17. LIMITATION OF ABSTRACT	18. NUMBER OF PAGES	19a. NAME OF RESPONSIBLE PERSON
a. REPORT Unclassified	b. ABSTRACT Unclassified	c. THIS PAGE Unclassified			19b. TELEPHONE NUMBER (include area code)
			SAR	40	

CONVERSION TABLE

Conversion Factors for U.S. Customary to metric (SI) units of measurement.

MULTIPLY \longrightarrow BY \longrightarrow TO GET
 TO GET \longleftarrow BY \longleftarrow DIVIDE

angstrom	1.000 000 x E -10	meters (m)
atmosphere (normal)	1.013 25 x E +2	kilo pascal (kPa)
bar	1.000 000 x E +2	kilo pascal (kPa)
barn	1.000 000 x E -28	meter ² (m ²)
British thermal unit (thermochemical)	1.054 350 x E +3	joule (J)
calorie (thermochemical)	4.184 000	joule (J)
cal (thermochemical/cm ²)	4.184 000 x E -2	mega joule/m ² (MJ/m ²)
curie	3.700 000 x E +1	*giga bacquerel (GBq)
degree (angle)	1.745 329 x E -2	radian (rad)
degree Fahrenheit	$t_k = (t^{\circ}f + 459.67)/1.8$	degree kelvin (K)
electron volt	1.602 19 x E -19	joule (J)
erg	1.000 000 x E -7	joule (J)
erg/second	1.000 000 x E -7	watt (W)
foot	3.048 000 x E -1	meter (m)
foot-pound-force	1.355 818	joule (J)
gallon (U.S. liquid)	3.785 412 x E -3	meter ³ (m ³)
inch	2.540 000 x E -2	meter (m)
jerk	1.000 000 x E +9	joule (J)
joule/kilogram (J/kg) radiation dose absorbed	1.000 000	Gray (Gy)
kilotons	4.183	terajoules
kip (1000 lbf)	4.448 222 x E +3	newton (N)
kip/inch ² (ksi)	6.894 757 x E +3	kilo pascal (kPa)
ktap	1.000 000 x E +2	newton-second/m ² (N-s/m ²)
micron	1.000 000 x E -6	meter (m)
mil	2.540 000 x E -5	meter (m)
mile (international)	1.609 344 x E +3	meter (m)
ounce	2.834 952 x E -2	kilogram (kg)
pound-force (lbs avoirdupois)	4.448 222	newton (N)
pound-force inch	1.129 848 x E -1	newton-meter (N-m)
pound-force/inch	1.751 268 x E +2	newton/meter (N/m)
pound-force/foot ²	4.788 026 x E -2	kilo pascal (kPa)
pound-force/inch ² (psi)	6.894 757	kilo pascal (kPa)
pound-mass (lbm avoirdupois)	4.535 924 x E -1	kilogram (kg)
pound-mass-foot ² (moment of inertia)	4.214 011 x E -2	kilogram-meter ² (kg-m ²)
pound-mass/foot ³	1.601 846 x E +1	kilogram-meter ³ (kg/m ³)
rad (radiation dose absorbed)	1.000 000 x E -2	**Gray (Gy)
roentgen	2.579 760 x E -4	coulomb/kilogram (C/kg)
shake	1.000 000 x E -8	second (s)
slug	1.459 390 x E +1	kilogram (kg)
torr (mm Hg, 0 ^o C)	1.333 22 x E -1	kilo pascal (kPa)

*The bacquerel (Bq) is the SI unit of radioactivity; 1 Bq = 1 event/s.

**The Gray (GY) is the SI unit of absorbed radiation.

CONTENTS

Section	Page
Figures	iv
Tables	vi
1. Summary	1
2. Introduction	1
3. Geological and Geophysical Background	3
3.1 Geology and Tectonic Setting	3
3.2 Previous Geophysical Studies	3
4. Observed Receiver and Dispersion Response	6
4.1 Surface-wave Dispersion Observations	6
4.2 Receiver Function Estimates	7
5. Joint, Linearized Inversion With Constraints	9
5.1 Iterative Jumping Inversion Scheme	9
5.2 Additional Constraints For Upper Mantle Structure 11	
5.3 Upper Crust and Short-period Dispersion	13
6. Lithospheric Structure of the Arabian Shield	14
6.1. Afif Terrane	15
6.2 Asir Terrane	16
6.3 Nabitah Suture Zone	17
6.4 Inversion Results at RAYN	18
7. Discussion	19
8. Conclusions	21
9. Acknowledgments	22
10. References	22
Appendix	26
DISTRIBUTION LIST	DL-1

Figures

Figure		Page
1	Tectonic map of the Arabian peninsula showing the location of the 9 temporary stations in the Saudi Arabian Portable Broadband Deployment. Some permanent stations in nearby regions are shown, as well.	2
2	Love and Rayleigh wave group velocities (fundamental mode) from the tomographic inversion by Mokhtar et al. (2001) associated to the temporary stations in the Arabian Peninsula.	5
3	Azimuthal and slowness coverage of P-wave teleseismic sources for the temporary stations in the Arabian Peninsula. The radial coordinate corresponds to slowness, in steps of 0.025 s/km and the angular coordinate to backazimuth, in steps of 15°. The north direction points to the top of figure. The number of events displayed is indicated close to the station name.	8
4	Receiver function estimates for the temporary stations in Saudi Arabia at both low frequency ($f < 1.25$ Hz) and high frequency ($f < 0.5$ Hz). Top and bottom traces in each plot refer to radial and transverse receiver functions. When multiple traces are overlain, black refers to NE, dark gray to E and light gray to N. Traces are shifted for display purposes and the vertical amplitudes at RIYD are reduced by a factor of 2 to fit, as well.	10
5	Inversion results at station SODA using data only constraints and a half-space mantle. (a) receiver function predictions, (b) group velocity predictions and (c) preferred solution model. Solution model corresponds to $p=0.4$ and $\sigma=1.0$. Note the low velocity zone at the bottom of the model and the slow velocities in the near-surface structure.	12
6	Overlay of the data only inversion results for SODA (black), the inversion with constraints from Knox et al., (1998) model (dark gray), and the inversion with constraints from S12WM13 mantle model (gray). (a) receiver function predictions, (b) group velocity predictions and (c) preferred solution model. Solution model corresponds to $p=0.4$ and $\sigma=1.0$. Note the trade-off between the upper mantle and the lower crust structures.	13

7	Comparison between the inversion with the full Love dispersion curve (black) and without the shortest periods (dark gray) at station SODA. The near-surface velocity values are closer to those inferred in Mokhtar et al. (1988). Note the different upper crust structure obtained with this new data set.	14
8	Inversion results corresponding to the stations located within the Afif terrane. The name of the station and the average backazimuth of the stack are indicated in the upper right corner of each receiver function plot. Solid and dashed lines correspond to observations and predictions, respectively.	16
9	Inversion results corresponding to the stations located within the Asir terrane. The name of the station and the average backazimuth of the stack are indicated in the upper right corner of each receiver function plot. Solid and dashed lines correspond to observations and predictions, respectively.	17
10	Inversion results corresponding to the stations located within the Nabitah suture zone. The name of the station and the average backazimuth of the stack are indicated in the upper right corner of each receiver function plot. Solid and dashed lines correspond to observations and predictions, respectively.	18
11	Inversion results corresponding to station RAYN located in the Ar-Rayn terrane. The name of the station and the average backazimuth of the stack are indicated in the upper right corner of each receiver function plot. Solid and dashed lines correspond to observations and predictions, respectively.	20
12	Comparison of the Mooney et al. (1985) (solid gray), Prodehl (1985), (dashed gray) and Badri (1990) (dotted gray) interpretive crustal sections with the NE inverted models from the joint inversion (solid black).	21
13	Comparison of the Sandvol et al. (1998) crustal thicknesses (circles) and the crustal thicknesses inferred from the joint inversion (squares).	22

Tables

Table		Page
A1	Receiver function stack parameters	26
A2	Afif terrane S-wave velocity models	27
A3	Asir terrane S-wave velocity models	28
A4	Nabitah suture zone S-wave velocity models	29
A5	Structures sampled by station RAYN	30

Lithospheric structure of the Arabian shield from the joint inversion of receiver function and surface-wave dispersion observations

Jordi Julià, Charles J. Ammon, and Robert B. Herrmann

1. Summary

We estimate lithospheric velocity structure for the Arabian shield by modeling receiver functions and Love and Rayleigh group velocities from events recorded by the 1995-1997 Saudi Arabian Portable Broadband Deployment. Receiver functions are primarily sensitive to shear-wave velocity contrasts and vertical travel times and surface-wave dispersion measurements are sensitive to vertical shear-wave velocity averages, so that their combination bridges resolution gaps associated with each individual data set. We incorporate depth-dependent smoothness constraints on the resulting velocity models utilizing a jumping inversion technique. Additional constraints for the upper mantle are placed during inversion to complement those provided in our data set. Our results show a 32-36 km thick crust consisting of a 10-12 km thick upper crust containing a rapid velocity increase, a rather constant velocity lower crust of 3.84 ± 0.04 km/s overlain by a significant velocity gradient above 16-22 km depth. The upper mantle material is shown to have shear velocities ranging from 4.3 to 4.6 km/s and the crust-to-mantle transition is imaged as a gradational transition zone (4-12 km thick) rather than a sharp discontinuity. Evidence for lateral variations in both crust and upper mantle is observed at some stations, as well.

2. Introduction

A temporary network of broadband stations which recorded high-quality seismic signals was deployed in the Arabian Peninsula during 1996. The Saudi Arabian Portable Broadband Deployment (Figure 1) collected data that greatly improved the seismic coverage in the Arabian Peninsula, allowing new constraints on the lithospheric structure of that region and, therefore, originating new studies: Sandvol et al. (1998) computed receiver functions from P-wave teleseismic events to characterize first order discontinuities beneath the temporary network, Mellors et al. (1999) characterized regional phase propagation in the Arabian peninsula, Rodgers et al. (1999) estimated lithospheric velocity structure by modeling regional waveforms, and Mokhtar et al. (2001) used surface-wave records of events from along the plate margins to carry a tomographic study from dispersion measurements. In the present work, we obtain a shear-wave velocity structure for the Arabian Shield by simultaneously interpreting receiver function and surface-wave dispersion estimates.

The benefits of jointly inverting receiver function and surface-wave dispersion data have been shown by several authors Özalaybey et al. (1997), Du and Foulger, (1999), and Julià et al. (2000). When no noise is present, the complementary constraints in receiver functions and dispersion observations uniquely characterize the shear-wave velocity variation with depth, for a given set of layers with fixed thickness. Dispersion observations are sensitive to absolute vertical shear-wave velocity averages and the receiver functions

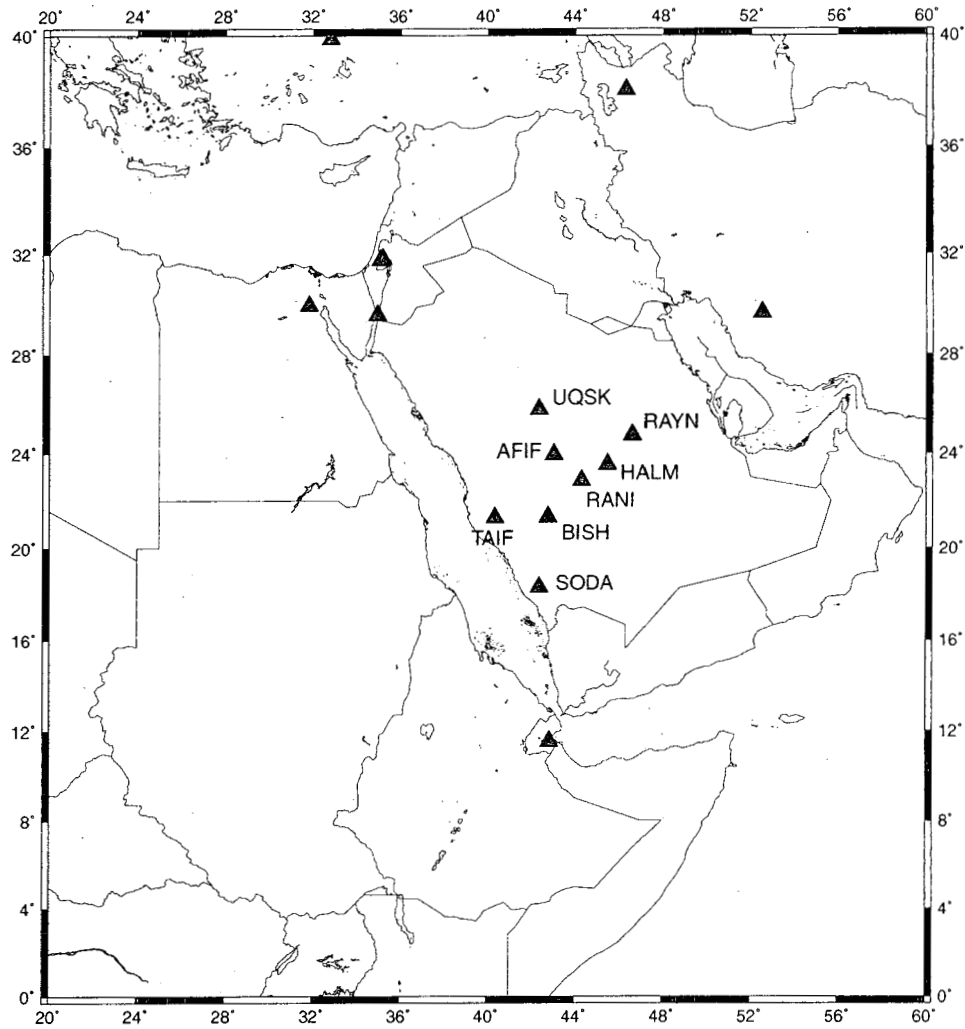


Fig. 1. Tectonic map of the Arabian peninsula showing the location of the 9 temporary stations in the Saudi Arabian Portable Broadband Deployment. Some permanent stations in nearby regions are shown, as well.

are primarily sensitive to shear-wave velocity contrasts and vertical travel times, so that their joint inversion gives rise to models where the details constrained by the receiver functions are superimposed on a background velocity model constrained by the dispersion measurements. When noise is contaminating the data, the constraints on the model parameters become incompatible, since the noise independently distorts the model imaged by both receiver function and dispersion measurements. (Julià et al., 2000). In this work we combine surface-wave dispersion data and receiver functions at overlapping frequency bands to constrain the shear-wave velocity structure in the Arabian Shield. Different frequency contents are considered simultaneously for the receiver functions to allow a better examination of the transition zones within the structure (Cassidy, 1992). It is also shown that the data only inversion does not suffice for the purpose of constraining the upper mantle structure and that additional constraints are required during the inversion process.

In the following we present and model receiver functions estimated in the Saudi Arabian Portable Broadband Deployment stations jointly with group velocities for the fundamental mode of Rayleigh and Love waves, as inferred from an independent tomographic study carried out by (Mokhtar et al., 2001). The receiver functions are obtained in this study by deconvolving the vertical trace of the teleseismic P-waveforms from its radial component to obtain receiver functions (Langston, 1979). Receiver function estimates at two overlapping frequency bands are inverted at the same time, jointly with the dispersion observations, to emphasize the first order structure beneath the recording stations. Our results show a simple crust for the Arabian Shield consisting of an upper, mid and lower crust structure overlying a crust-mantle transition. No evidence for upper mantle velocity contrasts, such as those imaged by (Sandvol et al., 1998). has been observed. The data allow analysis to be performed using waves approaching the stations at different backazimuths, and some evidence for lateral variations beneath some stations is suggested.

3. Geological and Geophysical Background

3.1 Geology and Tectonic Setting

The Arabian Peninsula is composed of the Arabian Shield and the Arabian Platform. The Arabian Shield attains the western one-third of the Arabian peninsula and is a composite of Precambrian and plutonic rocks (Brown, 1972). To the west, the Shield contains Tertiary and Quaternary volcanic rocks related to early stages of the Red Sea seafloor spreading system (Brown, 1972; Coleman, 1977). To the east, the Shield is bounded by the Mesozoic sedimentary rocks of the Phanerozoic Arabian Platform, which dip gently eastward and overlap the Shield unconformably (Powers et al., 1966). The platform consists of Paleozoic and/or Mesozoic and Cenozoic sedimentary rocks (Powers et al., 1966). The platform sediments thicken to the East and reach a 10 km thickness or more beneath the Mesopotamian foredeep (Brown, 1972) being relatively undeformed to the West.

The Shield is thought to have evolved from island arcs that formed during a series of subduction episodes and were subsequently juxtaposed by compressional orogenies (Schmidt et al., 1979). The Shield is split into five micro-plates: to the west, three intraoceanic island-arc terranes (Asir, Hijaz and Midyan), and to the east, one terrane of continental affinity (Afif) and one terrane of possible continental affinity (Ar Rayn), which are considered to be remnants of the Precambrian island arcs. These microplates are separated by four ophiolite-bearing suture zones of two types: the Bir Umq and Yanbu sutures, formed by island-arc-island-arc collision, and the Nabitah and Al-Amar sutures formed by arc-continent collision (Stoeser and Camp, (1985) To the SW the Asir terrane is bounded by the Hijaz-Asir escarpment.

3.2 Previous Geophysical Studies

A number of geophysical studies have been carried out in the Arabian Shield in order to investigate its crustal and upper mantle structure. These studies are based upon surface-wave dispersion measurements (Mokhtar and Al-Saeed, 1994; Ghalib, 1992; Mokhtar et al, 1988; Mokhtar et al, 2001; Rodgers et al., 1999), receiver functions (Sandvol et al.,

1998) and seismic refraction surveys (Mooney et al., 1985; Prodehl, 1985; Badri, 1991). Additionally, Ritzwoller and Levshin (1998) and Ritzwoller et al. (1998) produced tomographic maps from surface-wave group velocities across all of Eurasia, which are at a length scale intermediate between regional and global surface-wave studies.

Mokhtar and Al-Saeed (1994) modeled the shear-wave velocity structure of the Arabian Plate by inverting surface-wave dispersion measurements at RYD station (Figure 2). Their results suggest that the crust of the Arabian Shield consists of a 20 km thick upper layer with shear-wave velocity of 3.61 km/s which overlies a lower crust of similar thickness with a shear-wave velocity of 3.88 km/s. In the Platform, they infer an upper crust of 3.4 km/s and a lower crust of 4.0 km/s, with thicknesses comparable to those in the Shield. The upper mantle velocities are 4.6 km/s and 4.4 km/s for the Shield and the Platform, respectively. Ghalib (1992) used Rayleigh-wave fundamental-mode group-velocity observations from five analog stations to investigate the three-dimensional seismic structure of the Arabian Plate, reporting the presence of two discontinuities at 15-22 and 35-55 km depth. Mokhtar et al. (1988) derived the shear-wave velocity structure for the upper 1 km in different tectonic regions of the Arabian shield using high-frequency Rayleigh waves (1-20 Hz) recorded along a deep-refraction profile; they obtained the shear-wave velocities in the shield increases from 2.6 to 3.4 km/s in the upper 400 m of the crust. Mokhtar et al. (2001) present tomographic images for the Arabian Plate, constructed from average group velocity variations for both Love and Rayleigh waves. We use dispersion values contained in these tomographic images in our joint inversion.

Sandvol et al. (1998) estimated the lithospheric mantle and crustal velocity structures beneath the Arabian Shield through the modeling of teleseismic P waves recorded by the temporary network used in this study. Application of the receiver function technique showed that the crustal thickness beneath the coastal stations SODA and TAIF is 38.0 ± 1.0 km and 40.0 ± 2.5 km, respectively, the last estimation being within errors to station SODA. Beneath station RANI the crust is relatively thin (35.0 ± 2.5 km) and a Poisson ratio of 0.24 was required to fit the observations, in contrast to the 0.25 value used in all others. At the stations within the Arabian Shield (AFIF, HALM and RAYN) the crustal thicknesses were found to be 39.0 ± 1.0 km, 40.0 ± 1.0 km and 44.0 ± 2.5 km, respectively. Beneath the northernmost station UQSK the crust appears to thin to 37 ± 1.5 km. Station RAYN was the only one which required a major mid-crustal impedance contrast. They also observed sub-Moho velocity discontinuities beneath TAIF and HALM at about 90 km depth. The authors note that this is an unexpected result at TAIF since the lithosphere-asthenosphere boundary is thought to be at approximately 100 km depth along the Red Sea coast (Ghalib, 1992) with a negative velocity contrast. They also detect a similar contrast beneath RIYD and, unexpectedly, did not see any evidence for such a contrast beneath RAYN. Finally, a gradational increase in velocity beneath AFIF in the 60-70 km depth range is also suggested.

A large reversed refraction profile was conducted in 1978 across the Saudi Arabian Shield (Blank et al., 1979), and different interpretations were given by several authors. For example, Mooney et al. (1985) interpreted, to a first order of approximation, a P-wave velocity structure consisting of an upper crustal layer 20-21 km thick with an average

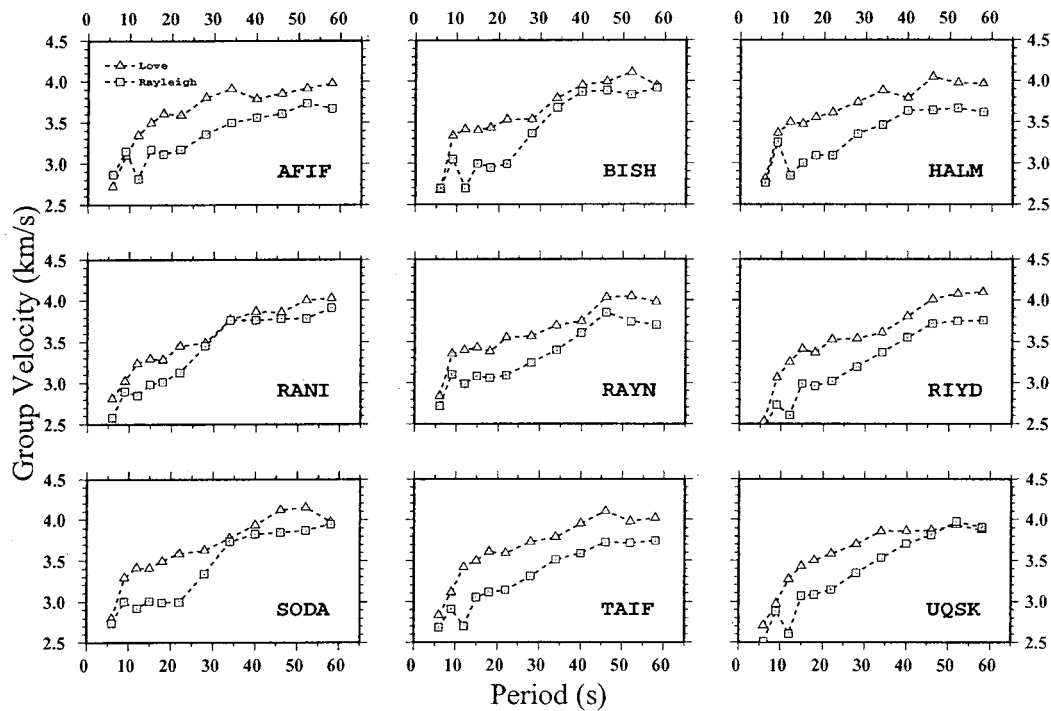


Fig. 2. Love and Rayleigh wave group velocities (fundamental mode) from the tomographic inversion by Mokhtar et al. (2001) associated to the temporary stations in the Arabian Peninsula.

velocity of 6.3 km/s, and a lower crustal layer 18-19 km thick with an average velocity of approximately 7.0 km/s. This is consistent with the S-wave velocity structure inferred by Mokhtar and Al-Saeed (1994). In the lowermost crust some evidence for lateral change in the velocity is found, although this is somewhat subjective. Higher gradients and correspondingly smaller velocity contrasts (7.8-8.0 km/s) at the Moho were found to the SW of the Nabitah suture zone and smaller gradients and higher velocity contrasts (7.3-8.1 km/s) were outlined to the NE. The crustal thickness varies from 38 km in the NE of the Shield to 43 km in the platform, and the velocities in the upper mantle vary from 8.0 km/s in the SW to 8.1 km/s in the NE. In addition they saw two first order velocity increases of 0.2-0.3 km/s and 0.2 km/s at a 60 km and 70 km depth, respectively.

A different interpretation based upon the same data set was provided by Badri (1991). His results contain an upper crust consisting of two layers: the first one with a velocity of about 6.08 km/s and 3 km thick in the shield, thinning to 1 km in the platform; the second one is about 6.2 km/s and 14 km thick in the shield, thinning to 7 km in the platform. The intermediate crustal layer has a velocity of 6.43 km/s and about 7.5 km thick in the shield, and 6.38 km/s and 16 km thick in the platform. The lower crust is about 6.85 km/s and 15 km thick. He also reports lateral variations in the location in depth of the boundaries between the crustal layers and the crust-mantle transition: the upper-lower

crust transition is 16.5 km depth between Afif and Al-Amar, 16.5-11.2 km beneath the Ar-Rayn terrane and 10 km beneath the platform; the crust-mantle transition is less than 40 km beneath the Afif terrane and Al-Amar suture zone, more than 40 km beneath the Ar-Rayn terrane and 42 km thick beneath the platform. The upper mantle velocity inferred in his analysis is 8.2 km/s in the platform and decreases to 8.15 km/s in the shield, and is characterized by the presence of strong positive velocity gradients.

Prodehl (1985) provided another interpretation based upon the same data set, which includes a crustal thickness of about 40 km for central Saudi Arabia and an upper mantle velocity of 8.2 km/s. He proposes an upper crust for the western Arabian Shield with relatively high-velocity material at about 10 km depth underlain by velocity inversions, and an upper crust for the eastern Shield that is relatively uniform. The lower crust is shown to have a velocity of about 7 km/s and the Moho beneath is shown not to be a first-order boundary but rather a transition zone, where the velocity increases from about 7.4 to 8.2 km/s in few kilometers.

Rodgers et al. (1999) modeled regional seismic waveforms recorded in the Saudi Arabian temporary array. For the Arabian Shield they obtained a 36 km deep Moho and average P- and S-wave crustal velocities of 6.42 and 3.70 km/s, respectively. Sub-Moho P- and S-wave velocities of 7.9 and 4.3 km/s were also inferred, suggesting a Poisson's ratio of 0.29 for the uppermost mantle of the Arabian Shield. For the Arabian Platform, the best-fitting model had a crustal thickness of 40 km, average velocities of 6.07 and 3.50 km/s for the P- and S-wave crustal velocities, respectively, and sub-Moho P- and S-wave velocities of 8.10 and 4.55 km/s, which correspond to a typical Poisson's ratio of 0.27 for stable continental regions.

Mellors et al. (1999) characterized regional waveform propagation in the Arabian Peninsula, and revealed a 8.0 ± 0.2 km/s P_n velocity, a 4.4 ± 0.2 km/s S_n velocity, and a 3.6 ± 0.2 km/s L_g velocity under the network.

4. Observed Receiver and Dispersion Response

From November 1995 thru February 1997 a temporary network of 9 broadband stations was deployed across the Arabian peninsula (Vernon and Berger, 1997). These stations were equipped with PASSCAL STS-2 seismometers and 24-bit REFTEK 72A-08 digitizers as acquisition units, with GPS timekeeping. All nine station sites proved to be exceptionally quiet and recorded high quality data. In this report we stack receiver functions estimated from teleseismic P-wave signals recorded in these stations and invert them for shear-wave velocity structure, jointly with local surface-wave dispersion measurements. A tomographic inversion carried out by Mokhtar et al. (2001) from regional signals recorded by the same network, provide the Love- and Rayleigh-wave group velocities used in this study.

4.1 Surface-wave Dispersion Observations

Mokhtar et al. (2001) measured surface-wave group velocities generated by earthquakes located along the boundaries of the Arabian plate in the Red Sea, Gulf of Aqaba, Gulf of

Aden, western Iran, Turkey, and the Dead Sea fault system. They compiled observations from four different sources: digital broadband seismograms from the Saudi Arabian 1996/1997 PASSCAL temporary seismic network, digital seismograms recorded by the permanent broadband stations in the region (1990 thru 1996), analog observations of Rayleigh waves from the regional WWSSN stations (1970 thru 1979) and analog observations from RIYD stations (1981 thru 1987). They performed single station measurements of group velocity applying the multiple filter analysis technique (Dziewonski et al., 1972; Herrmann, 1987). The dispersion measurements were obtained at each period in the range 5-20 s and at even periods only in the range 22-60 s. Observations from each period were inverted separately and the images from adjacent periods were averaged. Finally, they parameterized the regional slowness variations using a uniform, one-degree by one-degree grid of constant-slowness cells to produce group velocity maps by means of a conjugate-gradient least square algorithm (Paige and Saunders, 1982). The inclusion of measurements from a wide range of instruments and waveforms generated by events with varying location accuracy, as well as a period smoothing makes formal error uncertainties difficult to estimate. Throughout our analysis, we assume formal errors for the group velocities are approximately ± 0.05 km/s, for each period. One striking observation in these maps is the consistency of the results from both Rayleigh and Love waves. At the short periods, it is evident that the Arabian shield is characterized by relatively higher than average seismic velocity, while the Arabian platform is in general slower than the average velocity. For longer periods, the seismic velocity is higher in western Arabia than in eastern or northeastern parts of the plate.

Figure 2 shows the local surface-wave group velocities obtained from the tomographic inversion described above and used in this study. Each plot shows the group velocity values for the fundamental mode of the Love and Rayleigh waves corresponding to individual cells in tomography, each one of them containing the station site labeled at the bottom right corner. The dispersion curves are somewhat rough, a result of the period-by-period tomographic imaging, and in some instances the similar values of the Love and Rayleigh group velocities suggest other uncertainties at certain periods. Still, the values of the measurement are consistent with relatively simple structures, and although simple one-dimensional velocity structures will not match the detail in the observations, they will provide a smooth fit. The short-period observations at $T=5$ s are rare and strongly constrain the shallow structure; however, we found it more convenient to remove the shortest periods for Love waves ($T=5$ and 9 s) for the sake of consistency between our models and the shallow structure models obtained by Mokhtar et al. (1988). Finally, we note that the maximum period of 60 s limits the depth we can probe and, as shown below, our best constraints are on structure in the crust.

4.2 Receiver Function Estimates

To compute receiver functions we considered earthquakes recorded within the teleseismic distance range $30^\circ < \Delta < 90^\circ$ by the temporary network. Not every selected event was recorded by all of the stations in the network nor showed a good signal to noise ratio, thus providing different azimuthal coverage for station (Figure 3). We observe that the sources are primarily located northeast to east of the recording site, with few seismic

waves approaching the station from western or southern backazimuths. As a result, the P-wave codas used for receiver function computation sampled mainly the Arabian shield (the Arabian platform for RIYD) northeast to east of the stations.

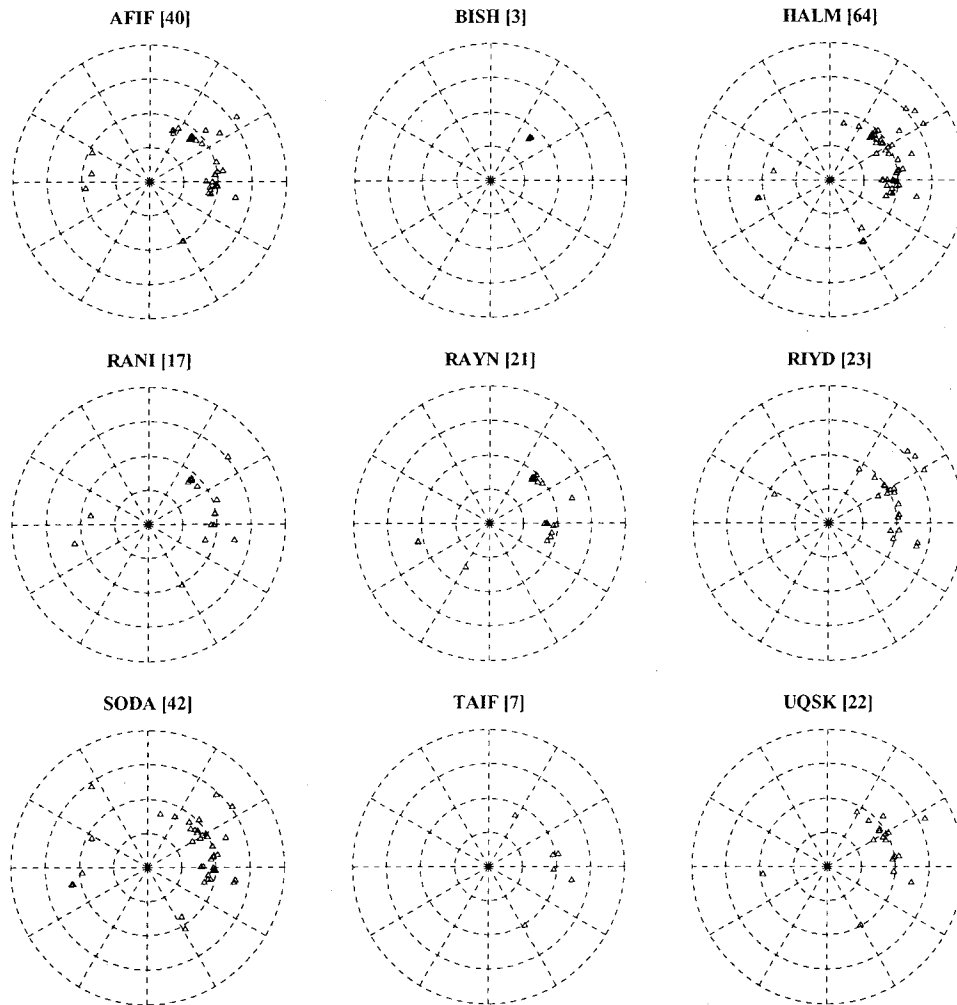


Fig. 3. Azimuthal and slowness coverage of P-wave teleseismic sources for the temporary stations in the Arabian Peninsula. The radial coordinate corresponds to slowness, in steps of 0.025 s/km and the angular coordinate to backazimuth, in steps of 15°. The north direction points to the top of figure. The number of events displayed is indicated close to the station name.

Receiver functions were obtained by deconvolving the horizontal traces of P-wave teleseismic records from the corresponding vertical trace (Langston, 1979). The time-domain iterative deconvolution technique introduced by Ligorria and Ammon (1999) was employed and radial and transverse receiver functions at high ($f < 1.25$ Hz) and low ($f < 0.5$ Hz) frequency bands were obtained for each event. We jointly invert both to give extra weight to the low-frequencies, which are less sensitive to the effects of small scale heterogeneities. To investigate the azimuthal dependence of the receiver response in the Arabian shield, we computed average receiver functions within tight backazimuth and ray parameter bounds at eastern backazimuths, overlapped the resulting waveforms,

and checked for coherency among the low-frequency traces. The bounds in ray parameter and backazimuth to be considered for stacking purposes depend on how the amplitude and timing of the converted and reverberated phases vary with lateral heterogeneity beneath the recording station (Cassidy, 1992). We found evidence for laterally varying structures beneath AFIF, RANI, RAYN, RIYD and UQSK, as described below. Stations BISH and TAIF did not provide enough coverage for such an investigation (Figure 3), but we note that SODA and HALM do, and that no significant variability in timing or amplitude was observed. Table A1 provides a summary of the ray parameter and backazimuth ranges employed in the final stacks.

Figure 4 gives an overlay of the radial and transverse average receiver functions used in our inversions (high and low frequency) throughout this study. The peak observed at in the radial waveforms near 5s is identified as the Ps converted phase from the Moho discontinuity, and the peak observed at around 15 s is identified as the PpPms reverberation throughout the crust. Differences in either amplitude (AFIF, RAYN) and timing (RANI, UQSK) are observed for these phases for a common station. A similar behavior is observed for some peaks and troughs between 5 and 15 s, which may correspond to crustal features (e.g. low velocity layers associated to the troughs) or, as suggested by Sandvol et al. (1998), to a Ps converted phase in the upper mantle. The transverse waveforms have amplitudes which are much smaller than the corresponding amplitudes in the radial trace. However, at stations RAYN, RIYD and RANI some significant transverse signal is observed northeast of the stations. This variability in the shape of the signals points to laterally varying structures within the Arabian shield and platform. Park and Levin (1999, AGU Abstract) succeeded in modeling some of the transverse observations with an anisotropic mantle lid, which should be kept in mind when interpreting our isotropic models.

5. Joint, Linearized Inversion With Constraints

In this work we invert the Love and Rayleigh group velocities jointly with the high and low frequency radial receiver functions to infer the shear-wave velocity in the crust and upper mantle of the Arabian shield. Former studies (Sandvol et al., 1998; Mooney et al., 1985) suggested upper mantle velocity changes beneath the Arabian Shield, so we invert for structure to a 100 km depth. In this section we will show that this poses some interesting problems in the inversion.

5.1 Iterative Jumping Inversion Scheme

We initially employed a "jumping" algorithm to jointly invert receiver functions and surface-wave observations for shear-wave velocity. The jumping scheme allows us to implement a smoothness constraint in the inversion by minimizing a model roughness norm (Constable et al., 1987) that can trade-off with the prediction error. The algorithm was successfully employed to invert receiver function data (Ammon et al., 1990), and to jointly invert receiver function and surface-wave dispersion data (Özalaybey et al., 1997; Du and Foulger, 1999). Our procedure also takes into account the different number of data points and different physical units of each data set, and incorporates an *a priori*

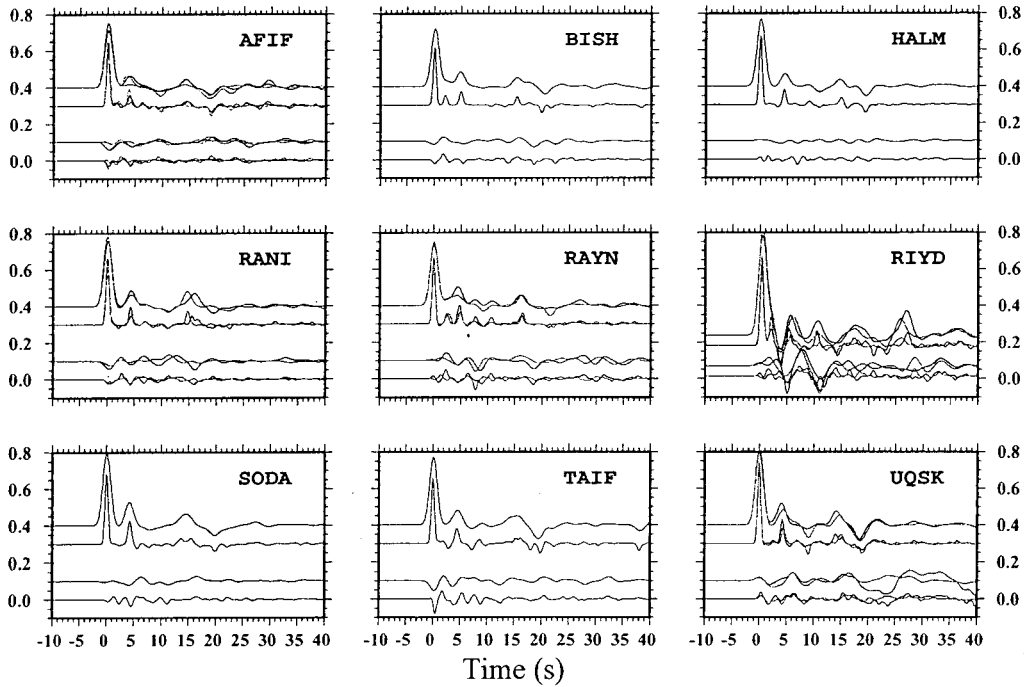


Fig. 4. Receiver function estimates for the temporary stations in Saudi Arabia at both low frequency ($f < 1.25$ Hz) and high frequency ($f < 0.5$ Hz). Top and bottom traces in each plot refer to radial and transverse receiver functions. When multiple traces are overlain, black refers to NE, dark gray to E and light gray to N. Traces are shifted for display purposes and the vertical amplitudes at RIYD are reduced by a factor of 2 to fit, as well.

parameter that allows to investigate the relative influence of each data set in the resulting models (Julià et al. 2000).

The system of equations to be inverted is given by

$$\begin{bmatrix} p\mathbf{D}_s \\ q\mathbf{D}_r \\ \sigma\Delta \end{bmatrix} \mathbf{m} = \begin{bmatrix} p\mathbf{r}_s \\ q\mathbf{r}_r \\ \mathbf{0} \end{bmatrix} + \begin{bmatrix} p\mathbf{D}_s \\ q\mathbf{D}_r \\ \mathbf{0} \end{bmatrix} \mathbf{m}_0 \quad (1)$$

where \mathbf{D}_s and \mathbf{D}_r are the partial derivative matrices for the dispersion measurements and the receiver function estimates, respectively, \mathbf{r}_s and \mathbf{r}_r are the corresponding vectors of residuals, \mathbf{m} is the vector of S-wave velocities, \mathbf{m}_0 is the starting model, and Δ is a matrix that constructs the second difference of the model \mathbf{m} . The partial derivative matrices and the vectors of residuals are normalized to equalize for the different number of data points and physical units in the data sets. A number of trade-off parameters must be specified before inversion. The influence factor, p , controls the trade-off between fitting receiver functions and dispersion curves, and the smoothness parameter, σ , controls the trade-off between data fitting and model smoothness. In (1) the parameter q is set to $q = 1 - p$, so that p is meaningless outside the range $0 \leq p \leq 1$. Our model parameters consists of

constant velocity layers of fixed thickness overlying a half-space, so that a one-dimensional interpretation of the earth structure is inferred.

As an initial test, Figure 5 displays the inverted model and the corresponding predictions at station SODA, obtained by jointly inverting Love and Rayleigh group velocities and high and low frequency receiver functions. Layers are 1 km thick in the 0-8 km depth range, 2 km thick up to 50 km depth and 5 km thick up to 100 km depth, where a half-space begins. The value for the trade-off parameters corresponding to the selected model are $p=0.4$ and $\sigma=1.0$, and have been chosen empirically, after a systematic study of the inversion results produced for a range of values, as indicated in Julià et al., (2000). The starting model is a 8 km/s P-wave velocity half-space, and the preferred solution consists of a simple layered crust overlying a crust-mantle transition zone. The low velocity zone at the bottom of the model is significantly low, especially for a shield region. Considering the period range of the surface-wave observations it is unlikely we can resolve much about the subcrustal structure. It would be easy to disregard the structure and focus on the crust. However, our observations are not independent of the deep structure, and to the extent that features at depth may trade off with crustal features, we would like to constrain our results to produce realistic mantle structures. The near-surface velocities are also extremely slow, with shear-velocity values well below the average 3.2 km/s inferred for the first kilometer from high-frequency Rayleigh waves (Mokhtar et al., 1988) in the shield.

5.2 Additional Constraints For Upper Mantle Structure

The extensive upper mantle low velocity zone in Figure 5 might be an artifact caused by the poor resolving power at depth of our data set. Additional *a priori* information could be required to stabilize the results. One possibility is to force the deepest layers in our model to be similar to predetermined values, such as those obtained from the inversion of intermediate period (20-60 s) surface-wave dispersion obtained by Knox et al., (1998), or from global mantle models like S12WM13 model (Su et al., 1994). This can be achieved by modifying (1) in the following manner (Jackson, 1972):

$$\begin{bmatrix} p\mathbf{D}_s \\ q\mathbf{D}_r \\ \sigma\Delta \\ \mathbf{W} \end{bmatrix} \mathbf{m} = \begin{bmatrix} p\mathbf{r}_s \\ q\mathbf{r}_r \\ \mathbf{0} \\ 0 \end{bmatrix} + \begin{bmatrix} p\mathbf{D}_s \\ q\mathbf{D}_r \\ \mathbf{0} \\ 0 \end{bmatrix} \mathbf{m}_0 + \begin{bmatrix} \mathbf{0} \\ \mathbf{0} \\ \mathbf{0} \\ \mathbf{W} \end{bmatrix} \mathbf{m}_a \quad (2)$$

where \mathbf{W} is a weighting matrix and \mathbf{m}_a is the *a priori* model.

Figure 6 compares the data only inversion and two different velocity constrained inversions for station SODA. The constrained inversions incorporate *a priori* estimates of mantle velocities for depths greater than 100 km and up to 500 km, and prohibit the receiver function data from constraining this part of the model to avoid wrap-around effects. The starting model up to 100 km depth and the parameters p and σ were identical to those used in the unconstrained inversion. We observe that the receiver functions are identical, and show good agreement with the data, and the predictions for the dispersion curves are identical up to 30 s period. We observe that the upper mantle velocities

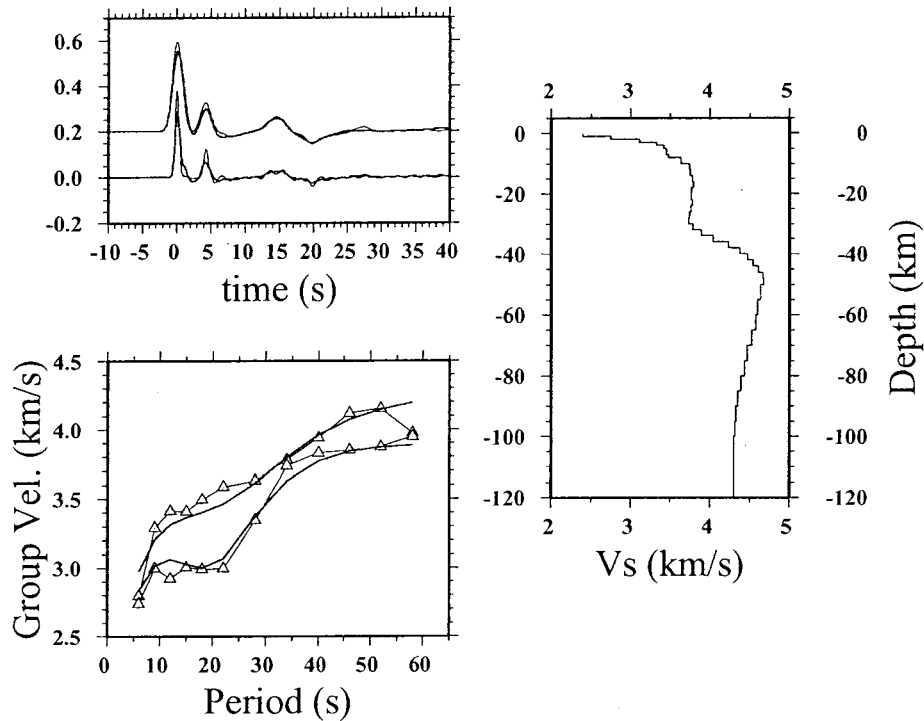


Fig. 5. Inversion results at station SODA using data only constraints and a half-space mantle. (a) receiver function predictions, (b) group velocity predictions and (c) preferred solution model. Solution model corresponds to $p=0.4$ and $\sigma=1.0$. Note the low velocity zone at the bottom of the model and the slow velocities in the near-surface structure.

obtained by the data only inversion are somehow slower than those obtained from the S12WM13 constrained inversion, and that the corresponding velocity values in the lower crust are slightly slower, as well. We also observe that the different upper mantle velocity values constrained by the Knox et al. (1998) values trade off with the lower crust velocity values (note the lower velocity at about 20 km depth). The important point is that although our data are not capable of resolving the deep structure they are sensitive to it, and that requiring our data to blend smoothly into an appropriate deep structure affects our estimate of the lower crust velocities.

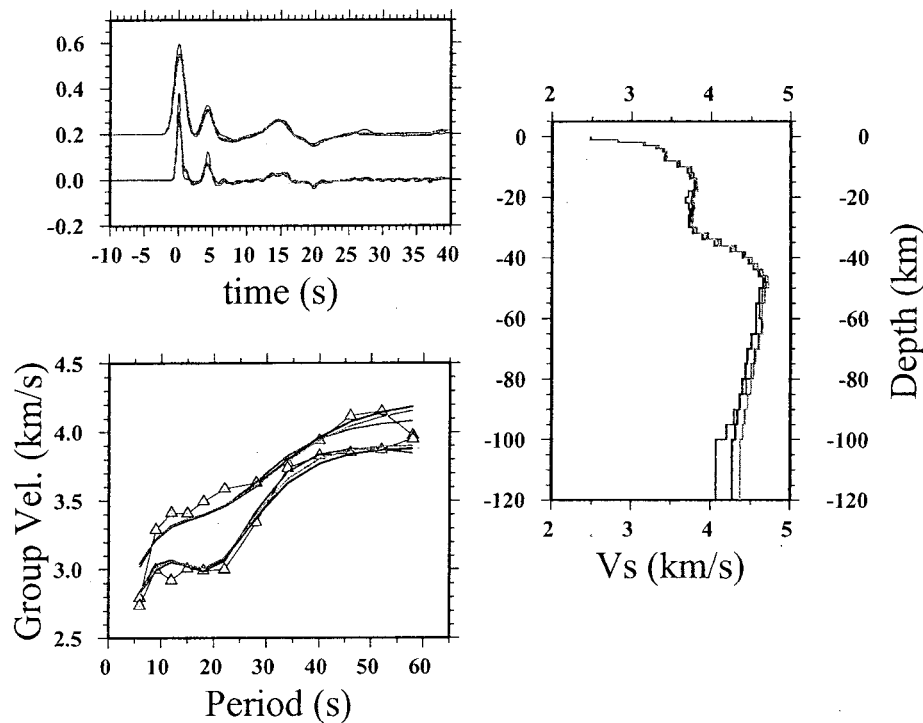


Fig. 6. Overlay of the data only inversion results for SODA (black), the inversion with constraints from Knox et al., (1998) model (dark gray), and the inversion with constraints from S12WM13 mantle model (gray). (a) receiver function predictions, (b) group velocity predictions and (c) preferred solution model. Solution model corresponds to $p=0.4$ and $\sigma=1.0$. Note the trade-off between the upper mantle and the lower crust structures.

We note that the fit to the Rayleigh velocity curve provided by the Knox et al. (1998) constraint values is excellent - as should be expected, since these mantle velocities were inferred from Rayleigh phase velocity measurements - but the fit to the longer periods in the Love curve are underestimated. Model S12WM13 provide a better compromise for both Rayleigh and Love group velocity measurements, and will be used throughout this study.

5.3 Upper Crust and Short-period Dispersion

The short-period dispersion observations provide strong constraints on shallow structure. Figures 5 and 6 have shown that the fit to the short periods provide extremely slow velocities in the uppermost crust, which contrast with the average 3.2 km/s that Mokhtar et al. (1988) inferred for the top 1 km depth from high-frequency (1-20 Hz) Rayleigh waves. To further investigate the effect of this short-period measurements we inverted receiver functions at SODA jointly with the group velocity values with the Love wave short periods (6 and 9 s) being removed. Figure 7 is a comparison of the inversion results thus obtained with the full dispersion curve inversion. In this case, a depth-dependent

smoothing was employed consisting of a $\sigma = 2.0$ for the top 8 km and $\sigma = 1.0$ for the remaining layers. We observe that the uppermost crustal velocity values are now compatible with those obtained from the high-frequency Rayleigh dispersion, and that the whole upper crust (top 12 km) has been affected by this removal of short period data.

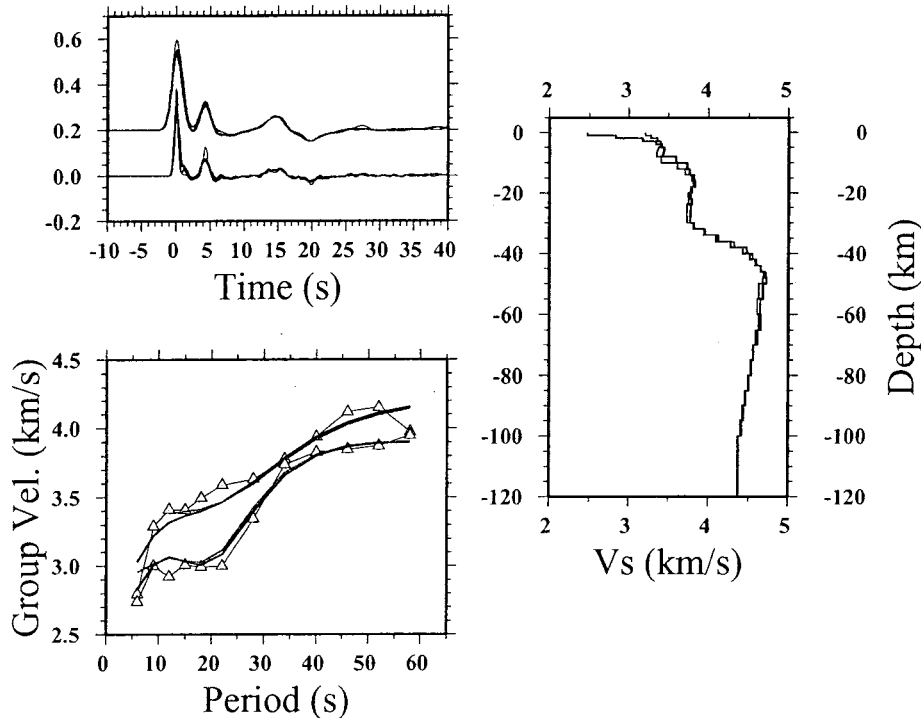


Fig. 7. Comparison between the inversion with the full Love dispersion curve (black) and without the shortest periods (dark gray) at station SODA. The near-surface velocity values are closer to those inferred in Mokhtar et al. (1988). Note the different upper crust structure obtained with this new data set.

6. Lithospheric Structure of the Arabian Shield

In this section we show the inversion results beneath the temporary stations in the Arabian shield. We employed the methodology described in the previous section, by performing several inversion suites for influence factors, p , of 0.2, 0.4, 0.6 and 0.8 at each station. In all cases we employed a depth dependent smoothing of $\sigma = 2.0$ for the top 8 km and $\sigma = 1.0$ for the remaining layers, which provided a reasonable balance between smoothness and fitting the observations. The best model was then selected by visual inspection after inversion. Two average receiver functions with different frequency content, $f < 0.5$ Hz and $f < 1.25$ Hz are inverted at the same time jointly with Love and Rayleigh fundamental mode group velocities for periods ranging from 12 to 56 s and 5 to 56 s, respectively. When possible, we also consider separate average receiver functions at different backazimuths (Table A1), to investigate any evidence of lateral heterogeneity. Inverting the same group velocity estimates jointly with azimuth varying receiver

functions may seem inconsistent; however, since dispersion curves just provide a large-scale background velocity model, we do not expect group velocities to be sensitive to slight lateral variations.

6.1 Afif Terrane

Figure 8 displays the inversion results for stations AFIF, HALM and UQSK, located in the Afif terrane, and Table A2 provides the velocity values for the inverted models. The Afif terrane is the only terrane of clear continental affinity located in the Arabian shield. The inverted models are strikingly simple and consist of 3-4 crustal layers overlying a gradational crust-mantle transition (CMT). Some upper mantle structure is observed beneath UQSK and AFIF, as well.

The upper crust extends to a 10-12 km depth and shows an apparent variability among models, even for the same station. Beneath AFIF and HALM, it consists of either a gradational velocity increase or a gradational increase overlying a constant velocity layer; beneath UQSK a low velocity layer (LVZ) is located between 5 and 10 km depth. The fit to the main peak in the receiver function is generally good, being clearly underestimated only for UQSK, and the short periods in the dispersion curves are generally overestimated. Both the P-wave amplitude and the short period group velocities constrain the shallow structure and, because of noise, it is difficult to find a unique value to match all observation. The lower crust is imaged as either a constant velocity layer with an average shear-wave velocity of 3.84 ± 0.04 km/s, or as a LVZ east of AFIF and UQSK. The signature of this LVZ is a clear trough at about 10 s. The upper and lower crust are connected by a significant gradient between 10 and 16 km depth.

The crust mantle transition (CMT) is sharp (4 km) and is located at 36 km depth beneath HALM and UQSK. At station AFIF it is located at 30-32 km depth, being 4-6 km thick.

Upper mantle velocities are 4.3-4.4 km/s at AFIF and HALM, and 4.5 km/s at UQSK, which are similar to those obtained by independent studies. Beneath UQSK some upper mantle structure consisting of a low velocity layer located between 40 and 55 km is observed. The upper bound is gradational, as it is observed in the 20 s trough in the low-frequency receiver function. This feature contributes to the fit to the peak and trough at 15 and 20 s, respectively, in the receiver function. More important, the Ps converted phase in the lower bound fits the feature located at 7 s in the receiver function, which was also interpreted as a Ps mantle conversion by Sandvol et al. (1998), but not modeled. Another possibility, not contemplated in our models, for interpreting the peak at 20 s is the Ps conversion at the 220 km discontinuity (Gurrola and Minster, 1998). Beneath the eastern models for AFIF an increase in velocity is suggested between 70 and 80 km, but no clear correlation to any Ps arrival is observed. Sandvol et al. (1998) observed a similar velocity increase beneath AFIF between 60 and 70 km, which is counterintuitive since they provide faster models. The northern AFIF model displays a broad LVZ in the uppermost mantle, which could be an attempt to model the trough at 20 s, as in UQSK.

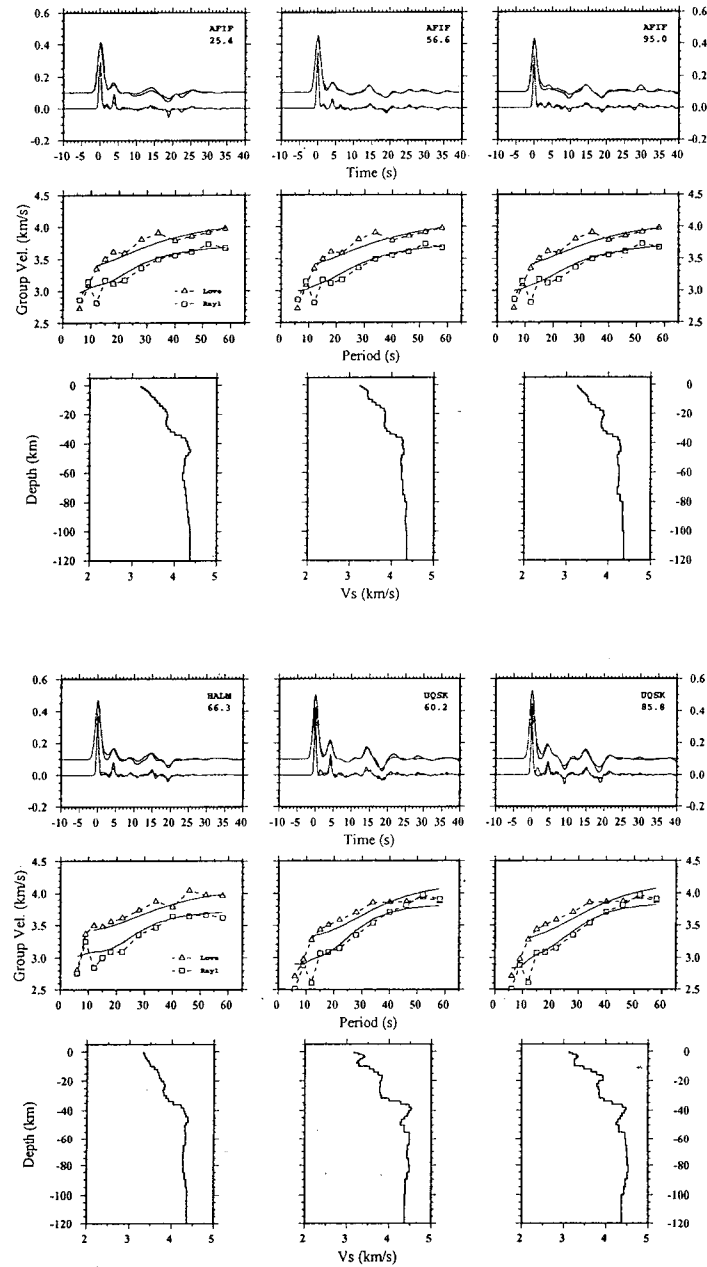


Fig. 8. Inversion results corresponding to the stations located within the Afif terrane. The name of the station and the average backazimuth of the stack are indicated in the upper right corner of each receiver function plot. Solid and dashed lines correspond to observations and predictions, respectively.

6.2 Asir Terrane

The two coastal stations, TAIF and SODA, provide information about the structure of the Asir terrane, which is one of the three intraoceanic island-arc terranes (Figure 9) and (Table A3). The crustal structures beneath these stations are very close to those inferred in the Afif terrane, although the transition between the upper and lower crust seems to be 2

km thinner. The CMT at TAIF is located at 34 km depth, is 8 km thick and increases in velocity up to 4.5 km/s. At SODA the CMT is located at 32 km depth and is 8 km thick, the lower bound being determined by a 4.5 km/s shear velocity cut-off.

As in UQSK, station TAIF shows a LVZ in the uppermost mantle associated to the pronounced trough at 20 s in the receiver function. The lower boundary of this LVZ, however, is more gradational since there is no clear peak right after this trough. Station SODA has the fastest uppermost mantle material when compared to the remaining stations, as required by the fast Rayleigh group velocities in the 35-45 s period range.

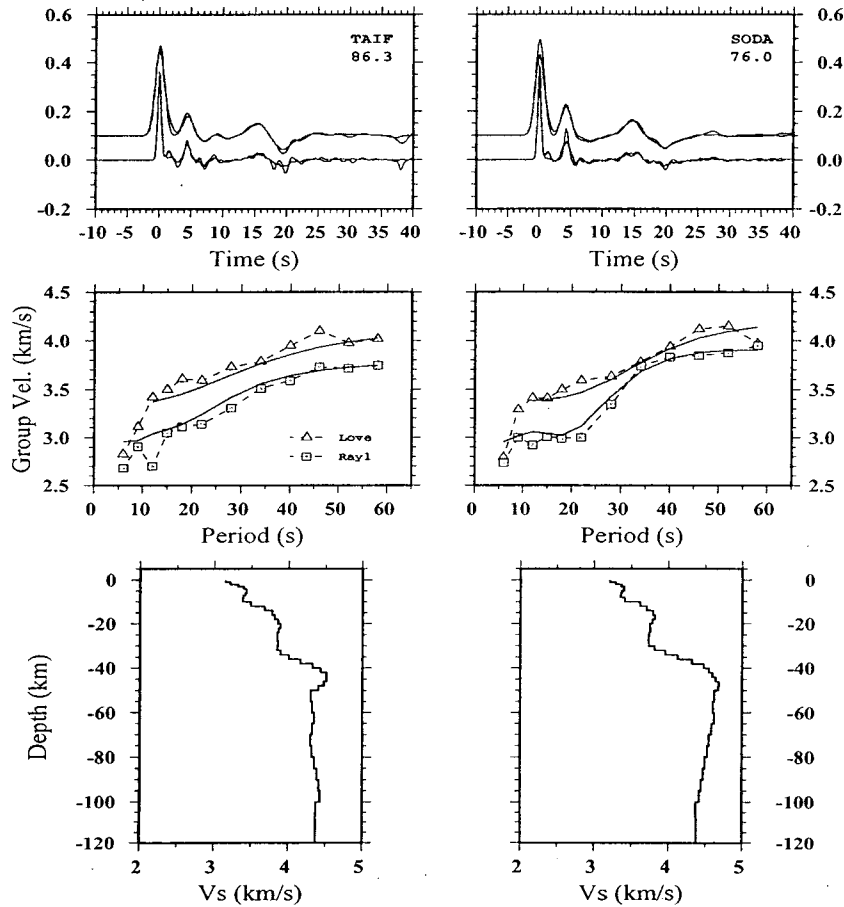


Fig. 9. Inversion results corresponding to the stations located within the Asir terrane. The name of the station and the average backazimuth of the stack are indicated in the upper right corner of each receiver function plot. Solid and dashed lines correspond to observations and predictions, respectively.

6.3 Nabitah Suture Zone

Stations RANI and BISH sample the subsurface structure of the Nabitah suture zone, which is of arc-continent collision type and separates the Afif and Asir terranes. Figure 10 and Table A4 provide the inversion results for these stations. The crustal structure is, again, similar to those inferred in the terrane stations. The upper crust extends to 8-10

km depth and consists of a gradational velocity increase overlying a rather constant velocity layer. The lower crust for the north-eastern structure at RANI is 3.91 km/s and turns to be a LVZ at eastern backazimuths. We note the excellent match in the 9-56 s period range for the dispersion curves at RANI, and that the lower and upper crusts are faster and slower, respectively, compared to those inferred in the terranes. The middle-lower crust boundary is difficult to discriminate beneath BISH, which shows a gradational velocity increase up to Moho depths. However, a lower crust of 3.90 km/s between 24 and 34 km depth is suggested.

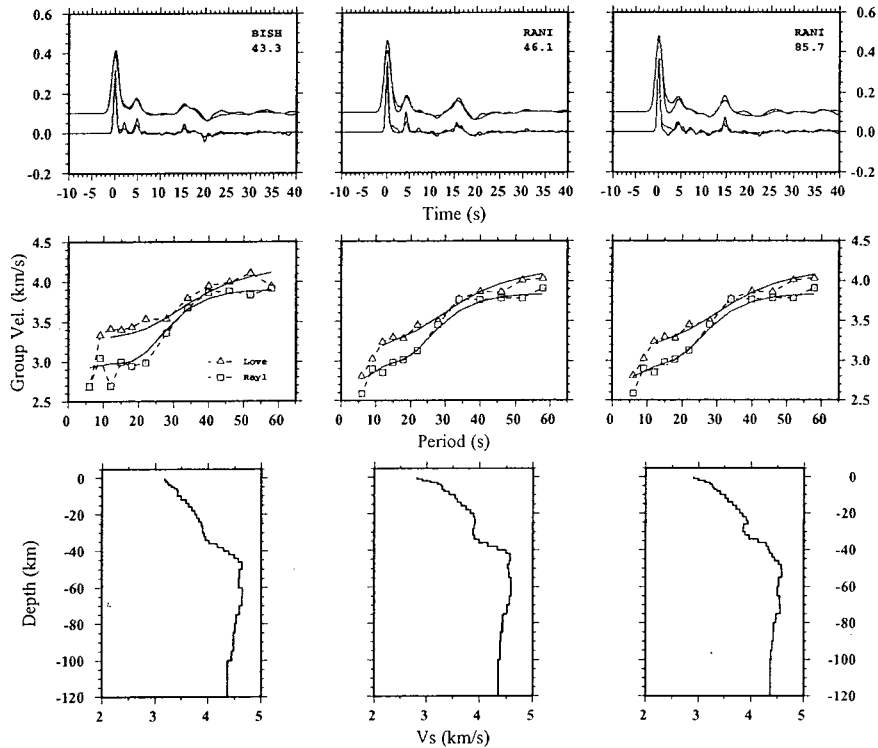


Fig. 10. Inversion results corresponding to the stations located within the Nabitah suture zone. The name of the station and the average backazimuth of the stack are indicated in the upper right corner of each receiver function plot. Solid and dashed lines correspond to observations and predictions, respectively.

The CMT is smooth beneath AFIF (12 km thick) and sharper northeast of RANI (8 km). Uppermost mantle velocities are over 4.5 km/s and no evidence for further structure is observed in any of the two stations.

6.4 Inversion Results at RAYN

Stations RIYD, located in the Arabian platform, and RAYN, located at the very eastern edge of the Ar-Rayn terrane, are theoretically sensitive to the structure of the platform. RIYD station has a very significant transverse component signal (see Figure 4), that prohibits any interpretation in terms of flat layers, so that we will focus on RAYN station.

The models obtained at RAYN (Figure 11, Table A5) show a strong azimuthal dependence. The lower crust velocities are similar (3.81 km/s and 3.84 km/s) but the middle crust is clearly slower for the northeastern model and the CMT location (34 km and 38 km) is clearly deeper for the eastern model. The PpPms multiple is located at 16 s for both directions, so that the deeper location of the CMT trades off with the faster mid-crust effect, keeping the travel time constant. Mokhtar and Al-Saeed (1994) inferred higher lower crust and slower upper crust velocities for the Platform respect to the Shield, as well as a thicker crust. Our inferred lower crustal velocities do not show it to be higher and the middle crust is clearly slower only at northeastern backazimuths. Conversely, only the eastern model has a clearly thicker crust. Station RAYN is just a single sample and, the fact that it does not provide an average image of this tectonic environment must be kept in mind. Upper mantle velocities lie between 4.4-4.5 km/s, which agrees with the values obtained in independent studies for the platform.

7. Discussion

We compare our northeastern models to the interpretive crustal sections provided by Mooney et al. (1985), Prodehl (1985) and Badri (1990) (Figure 12), where a Poisson's ratio of 0.25 has been assumed to plot shear-wave velocities. In general our upper crusts are slower than those inferred in any of the profiles. Our middle and lower crusts have a good agreement at HALM and RAYN with the models obtained by Prodehl (1985) but are dissimilar in the remaining stations. Attempting to explain those differences in terms of Poisson's ratio variation with depth would imply higher than 0.25 ratios in the upper crust and unlikely higher and lower than 0.25 ratio variations throughout the middle and lower crust. However a mean 0.25 Poisson's ratio for the middle and lower crusts seems reasonable. The CMT and the uppermost mantle imaged by our inversion are in excellent agreement with those inferred by Mooney et al. (1985) beneath SODA, BISH and RANI, but the sharp Moho discontinuity imaged in Mooney et al. (1985) and Badri (1990) beneath HALM and RAYN contrasts with our gradational CMTs. The PpPms reverberated phase, which gives a measure of the sharpness of the CMT, is generally well matched by our models in the low-frequency receiver functions, but it is seldom modeled in the high-frequency receiver functions, partly because of the bandwidth differences in long periods. None of the upper mantle contrasts imaged in the refraction surveys is observed in our models. The upper mantle velocities in our models are shown to be clearly slower, what we interpret as a consequence of the constraints imposed from S12WM13 model. If we combine the 8.0-8.1 km/s P-wave velocity in the refraction profiles with the 0.29 Poisson's ratio obtained by Rodgers et al. (1999) we obtain shear-wave velocities of 4.3-4.4 km/s, which are closer to our inferred values.

Another independent validation of our results can be done through a comparison with the receiver function modeling carried out by Sandvol et al. (1998). They employed a grid-search forward modeling technique to model receiver functions recorded by the same temporary array used in this study. As a result their models show an oversimplified crustal structure, but some interesting features are inferred, such as the crust-mantle boundary and some upper mantle structure. Figure 13 is a comparison of the crustal

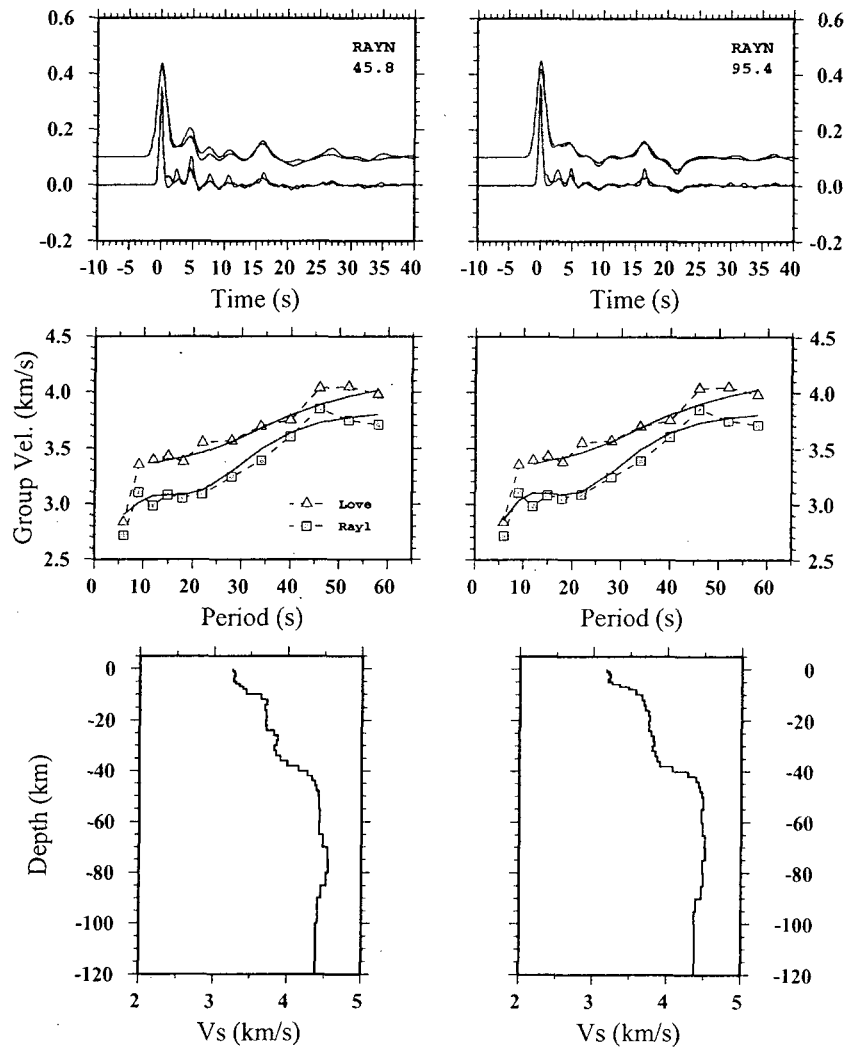


Fig. 11. Inversion results corresponding to station RAYN located in the Ar-Rayn terrane. The name of the station and the average backazimuth of the stack are indicated in the upper right corner of each receiver function plot. Solid and dashed lines correspond to observations and predictions, respectively.

thicknesses as inferred by Sandvol et al. (1998) to our estimates assuming the center of the CMT as the Moho. We observe that few of our estimates lie within their error bounds and that, in general, our estimated crusts are thinner. This could be a result of the well-known depth-velocity trade-off in receiver function studies: their models have faster crustal velocities, so that a thicker crust is needed to preserve the relative travel time of the phases modeled in the receiver function.

We could not find any evidence of the mantle velocity contrasts observed beneath HALM and TAIF at 90 km depth by Sandvol et al. (1998). Actually, the peaks that these authors interpret as a Ps conversion in the upper mantle are interpreted as a Ps conversion in the crust in our models.

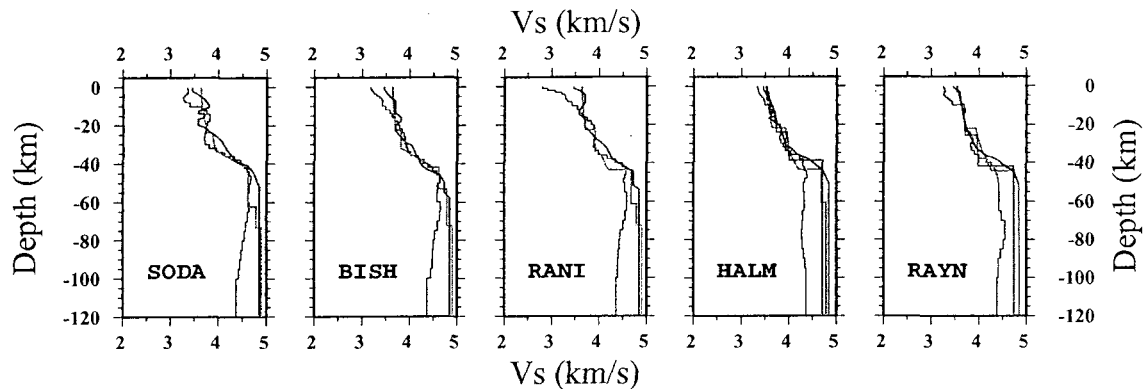


Fig. 12. Comparison of the Mooney et al. (1985) (solid gray), Prodehl (1985), (dashed gray) and Badri (1990) (dotted gray) interpretive crustal sections with the NE inverted models from the joint inversion (solid black).

8. Conclusions

All the models contain a rapid velocity increase during the few first kilometers below the surface, a lower crust with a rather constant velocity, and a gradational crust-to-mantle transition (CMT). The structures in the Afif and Asir terranes are similar and have faster and slower upper and lower crustal velocities, respectively, when compared to the structure obtained for the Nabitah suture zone. In most of the stations a mid-to-lower crust second order boundary, consistent with that inferred from independent works is inferred at 16-22 km depth, as well. A rather constant velocity (3.84 ± 0.04 km/s) lower crust is observed at all the stations, which is consistent with the value obtained by Mokhtar and Al-Saeed, (1994). The eastern models for RANI, AFIF and UQSK show an LVZ in this part of the crust, though.

The crust-mantle transition location ranges between 32 and 36 km depth at all the shield stations, and is deeper for the eastern RAYN model. Previous works estimated upper mantle velocities in the shield that range from 4.3 to 4.6 km/s for the shield mantle material. We found upper mantle velocities within this range in our models, that gives CMT thickness within 4 and 12 km depth range. Further verification of the inferred CMT thicknesses could be obtained from $P_s/P_p P_m$ s amplitude ratios (Ligorria, 2000). The northwestern stations UQSK, AFIF and TAIF show evidence for a LVZ in the top of the upper mantle.

We also show that the combination of receiver functions and short-period dispersion curves cannot unambiguously resolve the fine structure of the upper mantle. Independent information must be provided during the inversion process to insure a reasonable upper mantle in the model, since allowing the inversion to place an unlikely structure affects the estimates of the lower crust velocities. These additional constraints could be masking upper mantle structure inferred in independent studies, but our results show that upper mantle structure is not required to fit the observations.

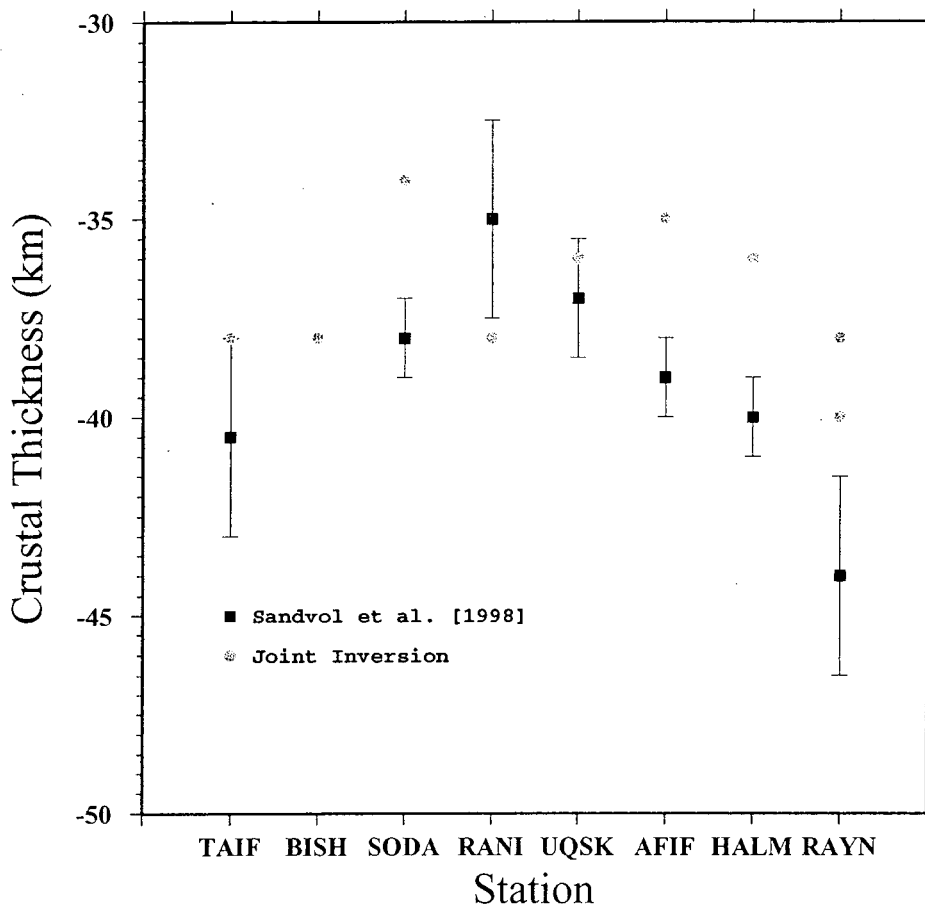


Fig. 13. Comparison of the Sandvol et al. (1998) crustal thicknesses (circles) and the crustal thicknesses inferred from the joint inversion (squares).

9. Acknowledgments

Generic Mapping Tools (Wessel and Smith, 1995) were used the figures in this paper.

10. References

Ammon, C. J., G. E. Randall, and G. Zandt, On the nonuniqueness of receiver function inversions, *J. Geophys. Res.* 95, 15303-15318, 1990. (UNCLASSIFIED)

Badri, M., Crustal structure of central Saudi Arabia determined from seismic refraction profiling, *Tectonophysics*, 185, 357-374, 1991. (UNCLASSIFIED)

Blank, H.R., J.H. Healy, J. Roller, R. Lamson, F. Fischer, R. McClearn, and S. Allen, Seismic refraction profile, Kingdom of Saudi Arabia - Field operations, instrumentation, and initial results, Saudi Arabia Mission Proj. Rep. 259, 49pp., U.S. Geol. Surv., 1979.

(UNCLASSIFIED)

Brown, G. F., Tectonic map of the Arabian Peninsula, scale 1:xx,xxx, Saudi Arabian Dir. Gen. Miner. Resour. Saudi Arabian Peninsula Map AP-2, 1972. (UNCLASSIFIED)

Cassidy, J.F., Numerical experiments in broadband receiver function analysis, Bull. Seism. Soc. Am., 82, 1453-1474, 1992. (UNCLASSIFIED)

Coleman, R. G., Ophiolites. Ancient Oceanic Lithosphere ?, 229 pp., Springer-Verlag, Berlin, 1977. (UNCLASSIFIED)

Constable, S.C., R.L. Parker, and C.G. Constable, Occam's inversion: A practical algorithm for generating smooth models from electromagnetic sounding data, Geophysics, 52, 289-300, 1987. (UNCLASSIFIED)

Du, Z.J. and G.R. Foulger, The crustal structure beneath the northwest fjords, Iceland, from receiver functions and surface waves, Geophys. J. Int. 139, 419-432, 1999. (UNCLASSIFIED)

Dziewonski, A.M. and A.L. Hales, Numerical analysis of dispersed seismic waves, in Methods in Computational Physics, edited by B. Alder, S. Frenbach and M. Rotenberg, pp. 39-85, Academic Press, New York, NY, 1972. (UNCLASSIFIED)

Ghalib, H. A. A., Seismic velocity structure and attenuation of the Arabian plate, PhD. Thesis, 350 pp., Saint Louis University, 1992. (UNCLASSIFIED)

Gurrola, H., and B. Minster, Thickness estimates of the upper-mantle transition zone from bootstrapped velocity spectrum stacks of receiver functions, Geophys. J. Int. 133, 31-43, 1998. (UNCLASSIFIED)

Herrmann, R.B., (Ed.). Computer Programs in Seismology, VOLI-III, Saint Louis University, Saint Louis, MO, 1987. (UNCLASSIFIED)

Jackson, D.D., Interpretation of inaccurate, insufficient and inconsistent data, Geophys. J. R. Astron. Soc., 28, 97-109, 1972. (UNCLASSIFIED)

Julià, J., C. J. Ammon, R. B. Herrmann, and A. M. Correig, Joint Inversion of receiver function and surface-wave dispersion observations, Geophys. J. Int. 143, 99-112, 2000. (UNCLASSIFIED)

Knox, R. P., A. A. Nyblade, and C. J. Langston, Upper mantle S velocities beneath the Afar and western Saudi Arabia from Rayleigh wave dispersion, Geophys. Res. Letters 25, 4233-4236, 1998. (UNCLASSIFIED)

Langston, C. A., Structure under Mount Rainier, Washington, inferred from teleseismic body waves, *J. Geophys. Res.* 84, 4749-4762, 1979. (UNCLASSIFIED)

Last, R. J., A. A. Nyblade, and C. A. Langston, Crustal structure of the East African Plateau from receiver functions and Rayleigh wave phase velocities, *J. Geophys. Res.* 102, 24469-24483, 1997. (UNCLASSIFIED)

Ligorria, J.P., An Investigation of the Crust-Mantle Transition Beneath North America and the Bulk Composition of the North American Crust, Ph.D. Thesis, xxx pp., Saint Louis University, 2000. (UNCLASSIFIED)

Ligorria, J.P. and C. J. Ammon, Iterative deconvolution and receiver function estimation, *Bull. Seism. Soc. Am.* 89, 1395-1400, 1999. (UNCLASSIFIED)

Mellors, R.J., V.E. Camp, F.L. Vernon, A.M.S. Al-Amri, and A. Ghalib, Regional waveform propagation in the Arabian Peninsula, *J. Geophys. Res.* 104, 20221-20235, 1999. (UNCLASSIFIED)

Mokhtar, T. A., R. B. Herrmann, and D. R. Russell, Seismic velocity and Q model for the shallow structure of the Arabian shield from short period Rayleigh waves, *Geophysics* 53, 1379-1387, 1988 (UNCLASSIFIED)

Mokhtar, T.A., Ammon, C.J., Herrmann, R.B., and Ghalib, H.A.A., Surface wave velocities across Arabia. *PAGEOPH* 158, 1425-1444, 2001. (UNCLASSIFIED)

Mokhtar, T. A., and M. M. Al-Saeed, Shear wave velocity structures of the Arabian Peninsula, *Tectonophysics*, 230, 105-125, 1994. (UNCLASSIFIED)

Mooney, W. D., M. E. Gettings, H. R. Blank, and J. H. Healy, Saudi Arabian seismic-refraction profile: A travelttime interpretation of crustal and upper mantle structure, *Tectonophysics*, 111, 173-246, 1985. (UNCLASSIFIED)

Özalaybey, S., M. K. Savage, A. F. Sheehan, J. N. Louie, and J. N. Brune, Shear-wave velocity structure in the northern basin and range province from the combined analysis of receiver functions and surface waves, *Bull. Seism. Soc. Am.* 87, 183-189, 1997. (UNCLASSIFIED)

Paige, C.C. and M.A. Saunders, LSQR: An algorithm for sparse linear equations and sparse least squares, *ACM Trans. Math. Softw.*, 8, 43-71, 1982. (UNCLASSIFIED)

Powers, R.W., L. F. Ramirez, C. P. Redmond, and E. L. Elberg, Geology of the Arabian Peninsula-sedimentary geology of Saudi Arabia, Prof. Pap. 560-D, 147 pp., U. S. Geol. Surv., 1966. (UNCLASSIFIED)

Prodehl, C., Interpretation of a seismic-refraction survey across the Arabian Shield in western Saudi Arabia, *Tectonophysics*, 111, 247-282, 1985. (UNCLASSIFIED)

Ritzwoller, M. H. and A. L. Levshin, Eurasian surface wave tomography: Group velocities, *J. Geophys. Res.*, 103, 1839-1878, 1998. (UNCLASSIFIED)

Ritzwoller, M. H. and A. L. Levshin, Intermediate period group velocity maps across central Asia, western China, and parts of the Middle East, *Geophys. J. Int.*, 134, 315-328, 1998. (UNCLASSIFIED)

Rodgers, A.J., W.R. Walter, R.J. Mellors, A.M.S. Al-Amri, and Y.S. Zhang, Lithospheric structure of the Arabian shield and platform from complete regional waveform modeling and surface wave group velocities, *Geophys. J. Int.*, 138, 871-878, 1999. (UNCLASSIFIED)

Sandvol, E., D. Seber, M. Barazangi, F. Vernon, R. Mellors, and A. Al-Amri, Lithospheric seismic velocity discontinuities beneath the Arabian Shield, *Geophys. Res. Letters* 25, 2873-2876, 1998. (UNCLASSIFIED)

Schmidt, D. L., D. G. Hadley, and D. B. Stoeser, Late Proterozoic crustal history of the Arabian shield, southern Najd province, Kingdom of Saudi Arabia, evolution and mineralization of the Arabian-Nubian shield, *I.A.G. Bull.*, 3, 41-58, 1979. (UNCLASSIFIED)

Stoeser, D. B. and V. E. Camp, V.E., Pan-African microplate accretion of the Arabian shield, *Bull. Seism. Soc. Am.* 96, 817-826, 1985. (UNCLASSIFIED)

Su, W., R. L. Woodward, and A. M. Dziewonski, Degree 12 model of shear velocity heterogeneity in the mantle, *J. Geophys. Res.* 99, 6945-6980, 1994. (UNCLASSIFIED)

Vernon, F. and J. Berger, Broadband seismic characterization of the Arabian shield, Interim scientific and technical report, 17 pp, 1997. (UNCLASSIFIED)

Wessel, P. and W. H. F. Smith, New version of the Generic Mapping Tools released, *EOS Trans. AGU*, 76, 329, 1995. (UNCLASSIFIED)

Note: A revised version of this paper has been accepted for publication in *Tectonophysics* and is in press. The title and authors are the same. The published version of this paper is the preferred reference.

Appendix

Table A1. Receiver function stack parameters

Station	Num. Ev.	Dist. °	Baz °	dT/dΔ s/km
AFIF	5	94.5±4.1	25.4±01.7	0.041±0.002
	16	81.2±4.2	56.6±16.8	0.047±0.004
	11	84.1±5.3	95.0±03.9	0.046±0.003
BISH	3	87.4±0.0	43.3±00.1	0.042±0.001
HALM	44	81.8±3.7	66.3±21.7	0.047±0.004
RANI	5	85.8±0.7	45.1±03.6	0.044±0.001
	6	79.9±4.0	85.7±09.5	0.052±0.006
RAYN	9	82.4±0.9	45.8±03.2	0.046±0.001
	8	85.8±4.6	95.4±06.1	0.045±0.003
RIYD	8	77.2±4.3	59.3±06.0	0.049±0.004
	8	76.2±4.6	90.0±08.9	0.051±0.002
SODA	28	83.0±5.2	76.0±18.7	0.046±0.003
TAIF	4	79.2±2.2	86.3±06.4	0.049±0.002
UQSK	7	81.4±5.1	60.2±03.7	0.046±0.003
	8	78.6±2.4	85.8±05.0	0.049±0.002

Num.Ev.: number of receiver functions averaged at this distance and back azimuth

Dist: distance range for average

Baz: back azimuth range

dT/dΔ: spherical earth ray parameter

Table A2. Afif terrane S-wave velocity models

Lay.	Thick. km	AFIF	AFIF	AFIF	HALM	UQSK	UQSK
		25.4 km/s	56.6 km/s	95.0 km/s	66.3 km/s	60.2 km/s	85.8 km/s
1	1.0	3.20	3.25	3.26	3.33	3.17	3.13
2	1.0	3.24	3.29	3.28	3.34	3.27	3.20
3	1.0	3.30	3.35	3.31	3.35	3.38	3.30
4	1.0	3.35	3.40	3.34	3.36	3.42	3.34
5	1.0	3.39	3.43	3.37	3.39	3.37	3.30
6	1.0	3.41	3.43	3.41	3.42	3.30	3.26
7	1.0	3.42	3.42	3.45	3.45	3.26	3.25
8	1.0	3.46	3.42	3.48	3.47	3.24	3.25
9	2.0	3.52	3.45	3.51	3.49	3.28	3.26
10	2.0	3.59	3.53	3.53	3.59	3.53	3.48
11	2.0	3.65	3.62	3.59	3.65	3.64	3.65
12	2.0	3.72	3.74	3.69	3.69	3.75	3.78
13	2.0	3.78	3.82	3.80	3.70	3.83	3.93
14	2.0	3.82	3.85	3.88	3.74	3.82	3.94
15	2.0	3.84	3.85	3.89	3.80	3.79	3.83
16	2.0	3.82	3.84	3.86	3.83	3.80	3.79
17	2.0	3.80	3.84	3.84	3.82	3.78	3.83
18	2.0	3.81	3.82	3.83	3.79	3.78	3.85
19	2.0	3.84	3.84	3.84	3.81	3.80	3.84
20	2.0	3.90	3.88	3.88	3.87	3.82	3.86
21	2.0	4.01	3.97	3.96	3.92	4.00	3.96
22	2.0	4.16	4.12	4.10	4.03	4.28	4.16
23	2.0	4.27	4.25	4.24	4.21	4.49	4.40
24	2.0	4.30	4.28	4.27	4.28	4.53	4.48
25	2.0	4.32	4.26	4.28	4.30	4.47	4.45
26	2.0	4.35	4.27	4.29	4.33	4.44	4.40
27	2.0	4.37	4.29	4.29	4.38	4.37	4.35
28	2.0	4.33	4.29	4.24	4.39	4.30	4.29
29	2.0	4.27	4.24	4.21	4.34	4.27	4.25
30	5.0	4.24	4.23	4.23	4.31	4.37	4.32
31	5.0	4.22	4.24	4.26	4.33	4.48	4.46
32	5.0	4.19	4.23	4.26	4.33	4.48	4.48
33	5.0	4.24	4.26	4.25	4.29	4.44	4.50
34	5.0	4.26	4.27	4.22	4.28	4.42	4.50
35	5.0	4.28	4.32	4.29	4.27	4.47	4.51
36	5.0	4.30	4.35	4.35	4.28	4.49	4.53
37	5.0	4.31	4.35	4.34	4.31	4.44	4.50
38	5.0	4.34	4.33	4.34	4.34	4.40	4.46
39	5.0	4.36	4.35	4.34	4.36	4.38	4.43
40	---	4.37	4.37	4.37	4.36	4.37	4.37

A Poisson's solid is assumed to compute P-wave velocities.

Density related to P-wave velocity through $\rho = 0.32 V + 0.77$.

The back azimuth of the data used for the model is given beneath the station name.

Table A3. Asir terrane S-wave velocity models

Lay.	Thick.	TAIF	SODA
	km	86.3 km/s	76.0 km/s
1	1.0	3.15	3.21
2	1.0	3.21	3.28
3	1.0	3.31	3.36
4	1.0	3.39	3.40
5	1.0	3.42	3.39
6	1.0	3.43	3.37
7	1.0	3.41	3.35
8	1.0	3.38	3.35
9	2.0	3.38	3.40
10	2.0	3.48	3.61
11	2.0	3.68	3.70
12	2.0	3.78	3.79
13	2.0	3.81	3.81
14	2.0	3.85	3.77
15	2.0	3.89	3.74
16	2.0	3.86	3.75
17	2.0	3.84	3.73
18	2.0	3.85	3.72
19	2.0	3.85	3.73
20	2.0	3.84	3.81
21	2.0	3.88	3.96
22	2.0	4.00	4.13
23	2.0	4.16	4.32
24	2.0	4.33	4.48
25	2.0	4.43	4.55
26	2.0	4.51	4.60
27	2.0	4.51	4.65
28	2.0	4.48	4.68
29	2.0	4.41	4.68
30	5.0	4.31	4.63
31	5.0	4.32	4.61
32	5.0	4.35	4.62
33	5.0	4.32	4.59
34	5.0	4.30	4.55
35	5.0	4.31	4.53
36	5.0	4.35	4.50
37	5.0	4.38	4.47
38	5.0	4.41	4.45
39	5.0	4.43	4.42
40	---	4.37	4.37

Table A4. Nabitah suture zone S-wave velocity models

Lay.	Thick. km	BISH	RANI	RANI
		87.4 km/s	85.8 km/s	79.9 km/s
1	1.0	3.18	2.80	2.90
2	1.0	3.20	2.91	2.99
3	1.0	3.23	3.07	3.12
4	1.0	3.26	3.20	3.22
5	1.0	3.31	3.27	3.26
6	1.0	3.37	3.29	3.27
7	1.0	3.41	3.29	3.30
8	1.0	3.43	3.32	3.35
9	1.0	3.42	3.42	3.41
10	1.0	3.49	3.54	3.51
11	1.0	3.58	3.58	3.55
12	1.0	3.63	3.65	3.65
13	1.0	3.69	3.75	3.72
14	1.0	3.75	3.83	3.78
15	1.0	3.78	3.89	3.84
16	1.0	3.83	3.92	3.91
17	1.0	3.87	3.91	3.94
18	1.0	3.90	3.90	3.86
19	1.0	3.90	3.88	3.85
20	1.0	3.93	3.88	3.88
21	2.0	3.95	3.91	3.96
22	2.0	4.02	3.99	4.14
23	2.0	4.17	4.16	4.28
24	2.0	4.29	4.34	4.33
25	2.0	4.40	4.49	4.35
26	2.0	4.49	4.57	4.40
27	2.0	4.57	4.57	4.45
28	2.0	4.64	4.55	4.52
29	2.0	4.64	4.52	4.58
30	2.0	4.59	4.54	4.58
31	2.0	4.58	4.58	4.52
32	2.0	4.65	4.58	4.51
33	2.0	4.64	4.55	4.54
34	2.0	4.59	4.51	4.56
35	2.0	4.53	4.44	4.48
36	2.0	4.50	4.43	4.43
37	2.0	4.48	4.40	4.42
38	2.0	4.48	4.39	4.40
39	2.0	4.45	4.39	4.38
40	2.0	4.37	4.36	4.36

Table A5. Structures sampled by station RAYN

Lay.	Thick. km	RAYN	RAYN
		45.8 km/s	95.4 km/s
1	1.0	3.25	3.17
2	1.0	3.27	3.20
3	1.0	3.29	3.22
4	1.0	3.27	3.21
5	1.0	3.26	3.20
6	1.0	3.29	3.24
7	1.0	3.34	3.35
8	1.0	3.39	3.47
9	2.0	3.44	3.57
10	2.0	3.64	3.65
11	2.0	3.71	3.68
12	2.0	3.69	3.70
13	2.0	3.70	3.74
14	2.0	3.71	3.76
15	2.0	3.70	3.74
16	2.0	3.72	3.75
17	2.0	3.81	3.78
18	2.0	3.87	3.82
19	2.0	3.85	3.82
20	2.0	3.81	3.80
21	2.0	3.84	3.84
22	2.0	3.90	3.87
23	2.0	3.99	3.90
24	2.0	4.15	4.07
25	2.0	4.27	4.28
26	2.0	4.33	4.39
27	2.0	4.37	4.42
28	2.0	4.39	4.44
29	2.0	4.41	4.47
30	5.0	4.42	4.49
31	5.0	4.43	4.47
32	5.0	4.42	4.48
33	5.0	4.48	4.51
34	5.0	4.55	4.52
35	5.0	4.55	4.48
36	5.0	4.52	4.49
37	5.0	4.45	4.46
38	5.0	4.41	4.39
39	5.0	4.41	4.37
40	---	4.38	4.37

DISTRIBUTION LIST
DTRA-TR-03-26

DEPARTMENT OF DEFENSE

DEFENSE TECHNICAL INFORMATION CENTER
8725 JOHN J. KINGMAN ROAD,
SUITE 0944
FT. BELVOIR, VA 22060-0944
2 CYS ATTN: DTIC/OCA

DEFENSE THREAT REDUCTION AGENCY
8725 JOHN J. KINGMAN ROAD MS 6201
FT. BELVOIR, VA 22060-6218
2 CYS ATTN: TDND/ D. BARBER

DEPARTMENT OF DEFENSE CONTRACTORS

ITT INDUSTRIES
ITT SYSTEMS CORPORATION
1680 TEXAS STREET, SE
KIRTLAND AFB, NM 87117-5669
2 CYS ATTN: DTRIAC
ATTN: DARE

SAINT LOUIS UNIVERSITY
DEPARTMENT OF EARTH & ATMOSPHERIC
SCIENCES
3507 LACLEDE AVENUE
ST. LOUIS, MO 63103
ATTN: J. JULIA

